# Deformability-based separation of erythrocytes with deterministic lateral displacement

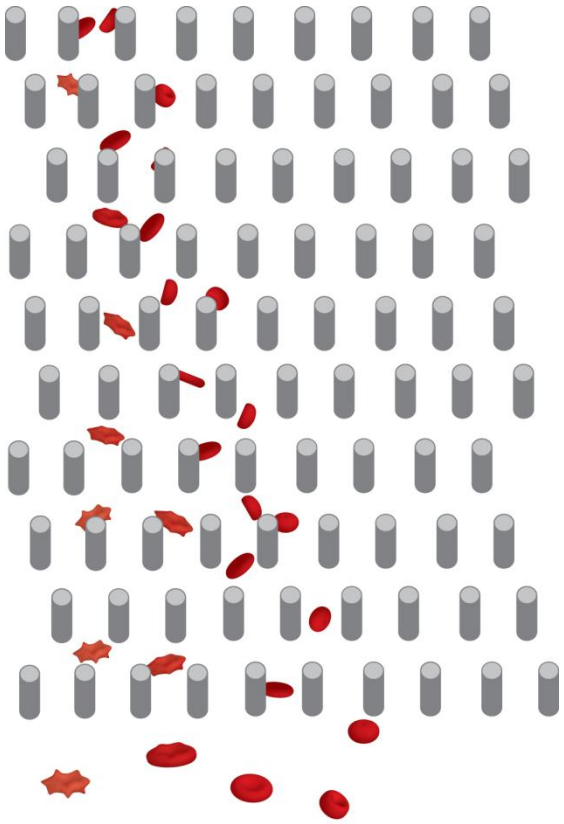

Author: Karl Adolfsson
Master thesis
Supervisors: Jason Beech and Jonas Tegenfeldt
Date: 2011-04-14
Department of solid state physics, Lund institute of technology

# Acknowledgements

I would like to thank Jason Beech, for showing me what it means to be a scientist, helping me whenever I asked (which was very often) and for inspiring me with his interesting ideas. Also, I want to thank Jonas Tegenfeldt for the much appreciated guidance and for letting me be a part of his research group and Stefan Holm who paved the way for me and was always eager to help.

More people I feel have helped me:
The bio group at solid state physics, for letting me practice rhetorics and the interesting discussions.
Bo Baldetorp, department of oncology, for teaching us basic flow cytometry and for letting us use their FACS
and lastly; Karin Lindström and my family for supporting me.

## Keywords

Deterministic lateral displacement, erythrocyte, red blood cells, deformability, microfluidics, cell sorting, anemia, blood disorders, diagnostics, biophysics, cell morphology, hematology, rheology.

## Summary

Discocytes and erythrocytes with (artificially induced) disease related morphologies were introduced in deterministic lateral displacement (DLD) devices of different depths and at varying shear rates, in order to evaluate DLD as a blood diagnostics tool.

Comparison with flow cytometry (FACS) results for corresponding erythrocyte morphologies indicate that the DLD can be used to study some equivalent cell indices and furthermore; DLD is able to discriminate based on parameters not visible in the FACS. Also, static velocity field particle simulations are presented as a tool to estimate some aspects of particle behavior in DLD devices.

# Contents

# 1 Introduction

The exciting field of microfluidics is likely to make many great contributions to biotechnology for a number of reasons. Advantages of downsizing fluidic reaction systems include less sample- and reagent volumes which means devices can be made cost efficient and several chemical reaction steps can be integrated on a single chip (*lab-on-a-chip)*. Also, other physical properties associated with the micro regime allow for working principles not possible in the macro world[1].

A promising aspect of microfluidics is the ability to separate small particles with high precision and resolution[2]. An example of where microfluidic separation techniques have already made a big impact is blood diagnostics and more specifically the flow cytometer (or automated counter) which was developed in the late 1960's by Bonner *et al*.[3] and came into practice in the 70's. Conventional flow cytometry, which is now commonplace in most hospitals, allows for digital analysis of erythrocyte indices based on single cell measurements (laser scattering) with high throughput and has arguably revolutionized clinical hematology. However, conventional flow cytometry is coupled with some drawbacks, and perhaps the most problematic aspect being that it is not portable or even accessible in large parts of the world (i.e. developing countries with poorly developed infrastructure). In addition, non-optically detectable abnormalities such as deformability are not measured, though decreased cell deformability has been identified as a symptomatic effect of many pathological states[4].

A promising candidate to complement the automated counter is the deterministic lateral displacement device (or DLD) first introduced by Richard Huang *et al*.[2]. The DLD is a passive sorting device, in that the separation principle does not require electronics or any other active components, and if it indeed proves to provide clinically relevant information, it would allow for a fast, cost efficient and mobile diagnostics tool to be used at point of care. Using a DLD device, the group of Robert Austin at Princeton University showed how whole blood could be continuously separated into its constituents of erythrocytes, leukocytes and plasma[5]. There are examples of DLD devices used in separating particles such as viral capsids, bacteria, parasites, fungal spores and more[6, 7], hence it is a very versatile separation method.

The results presented in this report reflect erythrocyte behavior in a DLD device (and that of some disease related erythrocyte morphologies) and how it is influenced by altering parameters such as device depth and shear force since these constitute some of the fundamental issues when considering DLD in blood diagnostics.

## 1.1 Abbreviations and constants

| | | |
|---|---|---|
| $p$ | Density | $kg\ m^{-3}$ |
| $\eta$ | Viscosity | $kg\ m^{-1}\ s^{-1}$ |
| $D$ | Diffusion coefficient | $m^2\ s^{-1}$ |
| $L, w, h$ | Channel length, width and height respectively | $m$ |
| $D_H$ | Hydraulic diameter | $m$ |
| $T$ | Temperature | $K$ |
| $P$ | Pressure | $Pa$ |
| $R$ | Hydrodynamic resistance | $Pa\ s\ m^{-3}$ |
| $v$ | Velocity | $m\ s^{-1}$ |
| $\gamma$ | Interfacial tension | $N\ m^{-1}$ |
| $\tau$ | Shear stress | $Pa$ |
| $\dot{\gamma}$ | Shear rate | $s^{-1}$ |
| $k_b$ | Boltzmann constant ($k_bT$ at room temp $\sim 4 \cdot 10^{-21} J$ ) | $\sim 1.38 \cdot 10^{-23} J\ K^{-1}$ |

# 2 Overview of the field

The developments and possibilities of microfluidics have inspired many to try to create cheaper, faster and more portable means for diagnostics and bio-applications in general. In this microfluidic regime, different physical properties have led to a new way of thinking where laminarity, diffusion and interfacial forces are fundamental building blocks which can be used to create complex biological or chemical systems which many believe will revolutionize the field of biotechnology.

## 2.1 Dimensionless numbers

Microfluidics may be characterized by dimensionless numbers that indicate what behavior dominates. An example is the Reynolds number which is the ratio between inertial- and viscous forces (see table 1) and for Re ≪ 2300 laminar flow will dominate over turbulent flow[2]. Other important numbers are the Peclét number which tell of particle- and device specific mixing by relating advection to diffusivity and the Capillary number which relates interfacial to viscous forces.

| Important dimensionless numbers and equations in microfluidics | |
|---|---|
| Reynolds number | $Re = \frac{inertial}{viscous} = \frac{pvD_H}{\eta}$ |
| Peclét number | $Pe = \frac{advection}{diffusivity} = \frac{Lv}{D}$ |
| Capillary number | $Ca = \frac{viscous}{interfacial} = \frac{\eta v}{\gamma}$ |
| Diffusion constant | $D = \frac{k_b T}{6\pi\eta a}$ |
| Mean diffusion length (3 Dim.) | $< r^2 >= 6Dt$ |

**Table1**. Equations and dimensionless numbers commonly used in microfluidics.

## 2.2 Components

Much effort has been focused on developing basic, enabling operations[8] such as mixing, separation, detection and driving principles which can be part of larger, more complex, systems. Microfluidics is generally dominated by laminar flow[8] (Re ≪ 1) which can be useful when it is desirable to preserve the integrity of fluid streams or plugs but poses a problem when fast mixing is required. Mixing principles mainly rely on diffusion with the general approach involving shortening diffusion lengths in various ways[8] (e.g. rotary mixers, magnetic mixers, chaotic advection mixers, bubble mixers and more).

Another characteristic of microfluidics is that when fluid velocity to diffusivity is high, fluid velocity profile is parabolic, resulting in smudged sample plugs and anisotropic particle velocities.

Like device materials, the means for driving fluid is closely linked to the characteristics of the device and like other aspects of microfluidics, many solutions have been realized (some of the common techniques are listed in table 3).

### 2.2.1 Separation

Essentially, separation involves forces acting asymmetrically on particles based on specific properties such as hydrodynamic diameter, dielectric properties, charge, affinity, diffusivity or indirect sorting based on automated feedback (e.g. FACS).

Many types of particles and containers have been introduced in microfluidic systems[2, 6, 7] (e.g. droplets, plugs, bacteria, virus

| Separation techniques in microfluidics | |
|---|---|
| Diffusion based | H-filter |
| Size/hydrodynamic size | FACS ,Deterministic lateral displacement (DLD) |
| Affinity | Antibodies, chemical affinity, MACS |
| Charge | Electrophoresis |
| Dielectric properties | Dielectrophoresis |
| Flow focusing | |
| Droplet tagging | Polystyrene beads in droplets |

**Table2.** Techniques for separating particles in microfluidics.

| Principles for driving fluids in microfluidics |
|---|
| Electrophoresis |
| Dielectrophoresis |
| Positive pressure |
| Negative pressure |
| Centrifugal |
| Gravitational |
| Capillary action |
| Wetting, electro-wetting |

**Table3.** The most common means for driving fluids in microfluidic devices.

capsules, various cell types and more) hence many different separation techniques have been introduced and the technique of choice depends on the setup. Interestingly separation techniques are exceptionally diverse and some common means of separation[8] are listed in table 2.

## 2.3 Materials and fabrication

Initially, silicon was the most commonly used device material, mainly because its use in microelectronics and consequently being a well-known material for micro fabrication. As an alternative, Xia and Whitesides proposed soft lithography with polydimethylsiloxane (PDMS) i.e. using a silicon master to produce multiple identical moldings in an elastomer[9]. This resulted in cheaper devices, less susceptible to breakage, and generally better suited for many applications. Soft lithography is currently one of the most common approaches for the reasons mentioned and due to the fact that PDMS is permeable to gas which is often desirable when dealing with biological samples such as cells. The pursuit of cheap and simple working-principles is an apparent trait of the microfluidics field and a prominent example of this mentality is the "paper-based" devices used in pregnancy tests which are now commonplace in supermarkets.

### 2.3.1 PDMS

Normally 10:1 PDMS to curing agent is mixed, poured on to a master and baked in 80 ℃ for about an hour. After the curing process, it is often treated with oxygen plasma to create superficial Si-OH groups which promote PDMS to glass (or PDMS) attachment and produce a hydrophilic surface.

Polydimethylsiloxane is an elastomer with many useful properties, such as gas permeability (as mentioned), transparency in the visible range (which allows for optical evaluation) and shrinkage of less than 1% after curing[9]. Another interesting feature of PDMS is its elastic nature, which allows for very dynamic device designs[19]. There are however some limitations in terms of width-to-height ratios to prevent channels from collapsing (due to its elastic/soft nature) and is therefore not suitable for all device designs.

### 2.3.2 PLL-PEG

To prevent cells and other complex samples from sticking to PDMS, a large compound known as poly-L-lysine-grafted poly-ethylene-glycol (PLL-PEG) is often used to coat the inner walls[10]. Adhesion to the electronegative surface (normally induced with oxygen plasma treatment) is facilitated by attraction of protonated amine functional groups of the lysine side chains in the poly-L-lysine backbone. The poly-ethylene-glycol serves as an anti-sticking agent by distancing sample molecules from the walls (i.e. as a *polymer brush*).

## 2.4 Bio applications of microfluidics

Many believe microfluidics will have a very big impact on diagnostics, in particular, which is consequently the focus of many research groups[2, 7, 11]. Much optimism is due to the possibilities in terms of portability and low costs in combination with new diagnostic principles. In developing countries where there is an unmet need for cheap diagnostics tools, these kinds of devices could prove particularly useful. Today, one of the most well-known diagnostics tools involving microfluidics is perhaps the flow cytometer[3] (and variations such as fluorescence activated cell sorting or FACS) which is found in large hospitals. Though it is normally not regarded as a microfluidics device in the current sense because of the complex and expensive setup which is difficult to implement in a portable format. That being said, microfluidics has yet to establish as a commercially successful industry in the biotech field.

For practical reasons, diagnostics is predominantly focused on easily

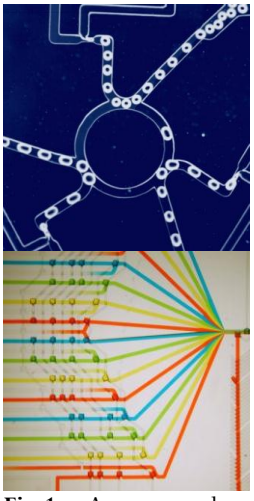

**Fig.1** An example of digital microfluidics (top)[i] and a microfluidic device with many valves and inlets (bottom)[ii].

[i]Courtesy of asst. prof. Manu Prakash Stanford university.
[ii]Courtesy of Folch lab, University of Washington, Seattle.

accessible entities such as blood and excretional substances though future systems might be more versatile. Many groups focus on blood because it is easily accessible and holds many parameters of clinical relevance.

Many methods involve separation without the use of specific markers[2, 7] (i.e. antibodies) which make devices cheaper and more versatile (though markers could of course be used as well).

Cell viability of isolated cells is especially valuable in order to study pharmaceutical effects on a specific cancerous species[12] and because microfluidics commonly involve in vivo like shear conditions, this kind of viable-cell-diagnostics hold great promise. Toner *et al*. have shown how rare (metastatic) circulating tumor cells (CTCs) could be detected at concentrations as low as 5 cells /ml whole blood, while maintaining viability using antibody-coated micro pillars in a laminar flow micro array[13].

Devices capable of detecting foreign bodies such as bacteria, virus and parasites have also been proposed. Holm and Beech *et al*. recently showed how sleeping sickness parasites (trypanosomes) could be isolated from whole blood based on hydrodynamic size with DLD[14].

Other promising areas of microfluidics is digital sequencing of genomes and proteomics[8, 11] where droplet fluidics (or *digital microfluidics*) in particular, is considered promising for cyclic reactions such as these (e.g. PCR) which involve many steps and high demand on precise quantities, fast thermal relaxation and sample integrity. Current techniques allow for formation of highly uniform droplets in the femtoliter regime at very high frequencies.

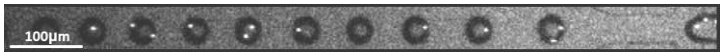


**Fig.2** Fluorescent polystyrene beads trapped in water-in-oil-droplets[iii].

[iii] An earlier project the author worked with in the experimental biophysics course (TEK265) at LTH.

# 3 Theory

## 3.1 Fundamental blood characteristics

Whole blood is composed of plasma, white blood cells, blood platelets and erythrocytes (red blood cells). The erythrocyte fraction, which comprises approximately half the blood volume (~45% for men and ~ 42% for women) and >99% of all blood cells[15], is called the *hematocrit* and is the focus of many blood diagnostics tests since erythrocytes play a central role in homeostasis. Erythrocytes are distinct from "normal cells" in that they have no nucleus (thus no genetic material) and few organelles, making them streamlined for the primary purpose of delivering oxygen to tissues and carbon dioxide back to the lungs. Erythrocytes contain the protein hemoglobin which is a hetero tetramer, each subunit containing a central ($Fe^{2+}$ -coordinating) *heme* group capable of associating one molecule of oxygen thus one hemoglobin complex can carry 4 molecules of oxygen in total[15].
Blood physiology has been extensively studied due to its importance and accessibility hence much is known about erythrocytes in comparison to most cells, and numerous pathological states have been characterized.

### 3.1.1 Blood pathology

The state of the blood (e.g. RBC morphology, chemical composition, presence of markers or bacteria etc) can at times tell a lot about the physiological state of an individual. As mentioned, a myriad of pathological states have been characterized and therefore only a fraction are mentioned in this report which focuses on a few of the diseases/abnormalities of erythrocytes, distinguishable with DLD.
Normally, cells that are less deformable or too large are diverted from the general blood stream when filtered through the red pulp of the spleen[iv] and individuals suffering from red blood cell alterations, consequently, lose red blood cells at a higher rate, resulting in anemia[16].
Pin-pointing red blood cell disorders commonly involves reticulocyte count, blood smears, hemoglobin levels, bone marrow biopsy and flow cytometry results such as mean corpuscular volume (MCV) and total cell count[17].
Reticulocytes, which are young erythrocytes with some remnant r-RNA and organelles, are larger than other erythrocytes and their relative presence can be very informative. High levels suggest that hematopoietic cells are responding to decreased erythrocyte levels and low levels indicate that the hematopoietic cells may have impaired functionality and are perhaps the underlying cause (*aplastic anemia*)[16]. Individuals suffering from anemia show symptoms related to the rate of erythrocyte loss e.g. hypovolemic shock if subjected to acute hemorrhage or other substantial blood losses and individuals with more slowly developing anemia tend to display symptoms like fatigue, pallor, dyspnea and more[16]. Disease states are either hereditary (such as sickle-cell anemia, hereditary spherocytosis etc), autoimmune or acquired e.g. by drugs, renal-liver failure, internal bleeding, malnutrition or mutations in hematopoietic cells. Some diseases associated with erythrocyte morphology are listed in table.4 and some corresponding blood smears can be seen in fig.4-8.

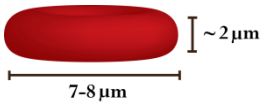


**Fig.3.** Dimensions of normal erythrocytes (mean values)[15].

| Some diseases associated with abnormal erythrocyte morphology | |
|---|---|
| Sickle-cell anemia | Autosomal co-dominant genetic disease (chromosome 11) |
| Echinocytosis | Liver disease, phosphate deficiency, hemolytic uremic syndrome and more. |
| Hereditary stomatocytosis | Autosomal dominant genetic disease (mutation in erythrocyte band 3 membrane protein) |
| Hereditary elliptocytosis | Autosomal dominant genetic disease |
| Thalassemia | Autosomal recessive genetic disease resulting in defect hemoglobin molecules. |
| Spherocytosis | Autosomal dominant genetic disease or some forms of autoimmune hemolytic anemia. |
| Microcytic anemia | Iron deficiency, drug-induced and more. |
| Macrocytosis | B12- or folic acid deficiency, liver failure, hypothyroidism. |

**Table 4.** Some known red blood cell diseases[16].

[iv] Senescent and less deformable erythrocytes are removed in the liver and bone marrow as well but to a lesser extent[16].

### 3.1.2 Bilayer-couple theory

The echinocytic-/stomatocytic transformations can be explained in terms of thermodynamics by considering energetically favorable states of different ratios of inner and outer membrane layer area[17, 18]. Normally $A_{inner}/A_{outer} \approx 0.98$ favoring the *discocyte* morphology but because of the narrow space between the layers (~3 nm) the favorable state is highly sensitive to changes in inner-outer leaflet ratio[17, 18]. Many amphiphilic compounds are known to be able to incorporate into either of the layers and it is believed that compounds with negatively charged moieties "prefer" the outer layer whereas compounds which can pass the membrane in an uncharged state prefer the inner layer. The echinocytic agent, sodium salicylate is known to transform approximately 86% (at ~30mM) of the erythrocyte population to echinocytes and triton X-100 is a potent stomatocytic agent[18]. Defect membrane proteins, such as *flippase*, which normally regulate the phospholipid composition of the leaflets and certain drugs, are also known to affect this ratio.

As the ratio between inner and outer layer changes, cells generally become more spherical (which is illustrated in fig. 9) and eventually lyse if distortion continues.

Factors such as osmolarity and pH can also change the morphology by changing cytosolic volume or chemical properties and create similar (almost identical) shapes as those produced by altering inner and outer leaflet area but the intrinsic viscosity is altered as well, in this case, and the leaflet ratio is believed to be unchanged (with respect to discocytes).

It is not fully clear as to whether this is the dominating mechanism underlying disease related transformations, however, and structural proteins such as *ankyrin* and *spectrin* are known to play major roles as well in maintaining the bi-concave discoid shape[18].

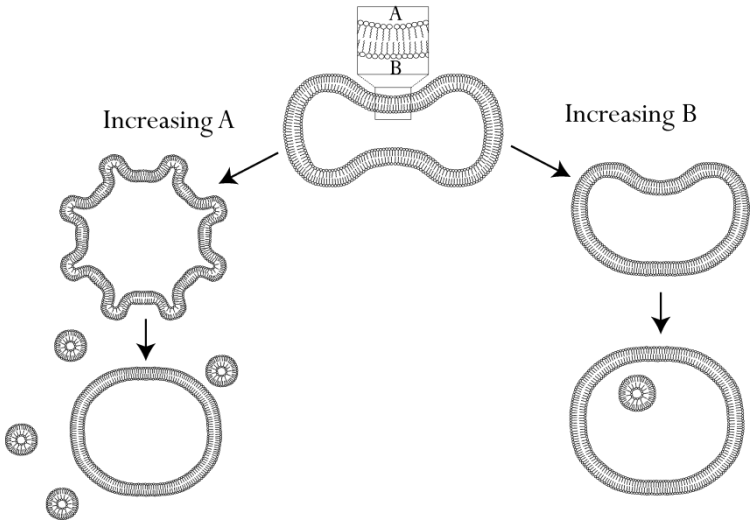


**Fig. 9.** Conceptual sketch of echinocytic- and stomatocytic transformation based on bilayer-couple theory[17, 18].

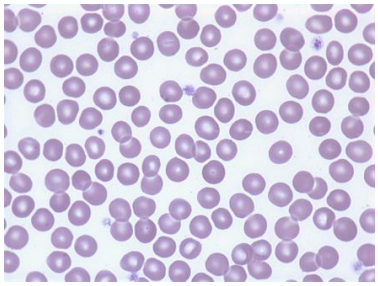

**Fig. 4** Normal erythrocytes[v].

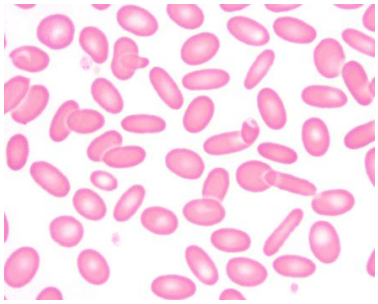

**Fig. 5** Hereditary elliptocytosis[v].

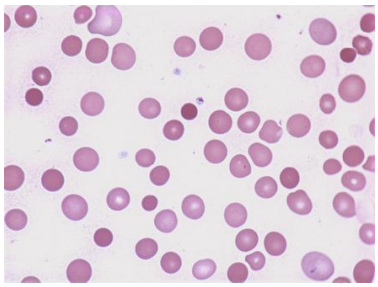

**Fig. 6** Hereditary spherocytosis[v].

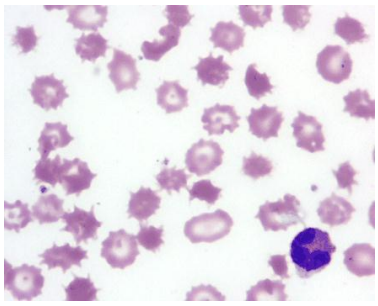

**Fig. 7** Echinocytosis[v].

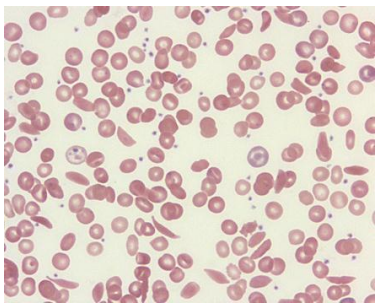

**Fig. 8.** Sickle cell anemia[v].

[v] American society of hematology image bank (ASH image bank).

## 3.2 Principles of deterministic lateral displacement

Deterministic lateral displacement is a separation technique discriminating between particles based on hydrodynamic size and/or deformability. Devices are composed of an array of posts (see fig. 10) in which each row is displaced a distance, $\Delta\lambda$, from the previous row resulting in a periodic row shift pattern if $N$ in eq. (1) is an integer

(1) $$N \cdot \Delta\lambda = \lambda.$$

Conservation of mass leads to the flow relation between the side and forward outlets in a unit cell as a function of period length, $N$, as

(2) $$Q_{side} = \frac{1}{N} Q_{forward}$$

where Q refers to volume flow ($m^3/s$). Particle behavior in the DLD array can largely be explained by considering $N$ different flow lanes in a unit cell of the array[2] (see fig. 11). Given the relation in eq. (2) a particle will exit the forward outlet, $N$-1 times, and the side outlet, 1 time, during a period of $N$ rows. In order to follow a flow lane a particle must "fit" in the lane, in other words, the center of the particle must be in the flow lane if the particle is to follow it (see fig. 12). The center of a spherical particle can never be closer to the post wall than its radius which leads to an approximate maximum radius for a rigid particle to fit in lane 1 as

(3) $$r_{max} \approx w_1$$

Particles with radii larger than $r_{max}$ will therefore not be able to exit the unit cell through the side outlet, and are, as a result, confined to lane 2 (in the case of $N = 3$). This is called *displacement mode* and results in a trajectory with a constant angle, $\theta$, related to the period and the distance between two laterally adjacent posts as $tan(\theta) = \frac{1}{N}$ with respect to the general flow and a total displacement (at the end of the array) equivalent to $n \cdot \Delta\lambda$ (where n is the total number of lateral rows). Particles with radii smaller than $r_{max}$, on the other hand, will go through all $N$ lanes during one period, resulting in a non-deviating trajectory in relation to the general flow. This is called the *zigzag mode* (the modes are visualized in fig. 13).

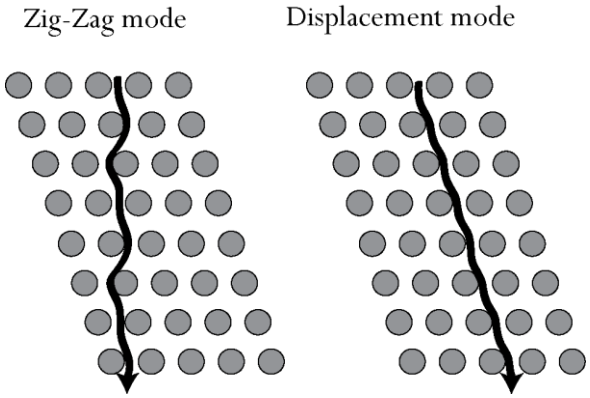


**Fig. 13** Trajectories or *modes* in which particles travel the DLD array.

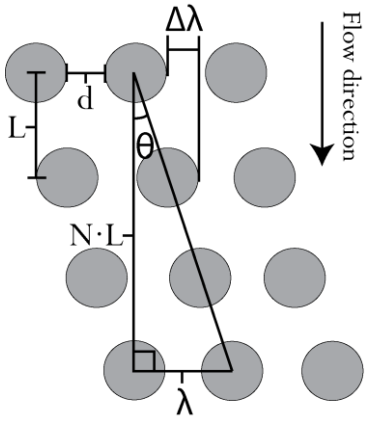


**Fig. 10.** Conceptual schematic illustrating important parameters of the DLD array.

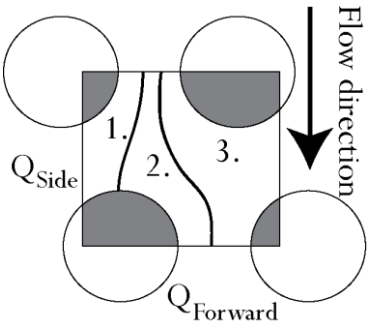


**Fig. 11.** A unit cell in the DLD array.

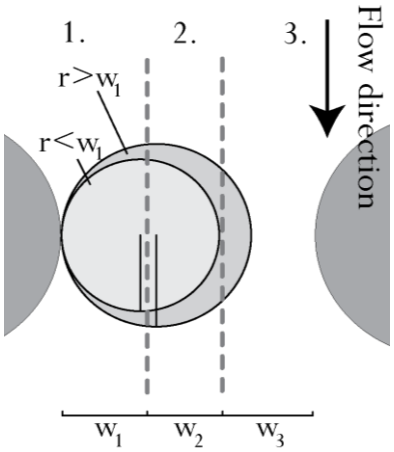


**Fig. 12.** The figure illustrates how particles of different size are confined to separate modes.

When dealing with irregular and/or deformable particles such as cells, many parameters influence the effective radius (or *hydrodynamic radius*) and in some cases it may change along the array (due to repeated plastic deformation). These factors may, in some cases, complicate separation in heterogeneous samples but can actually be utilized to discriminate between subpopulations when studying a seemingly homogenous population and it is the main topic of this report.

Soft particles deform when subjected to shear stress which, in the DLD, is largest between two laterally adjacent posts since shear stress $\propto \eta \frac{dv_y}{dx}$. Depending on the Young's modulus of a particle it will, to various extents, appear smaller in the DLD because the hydrodynamic radius decreases as it deforms (fig. 15 and fig. 16.B)

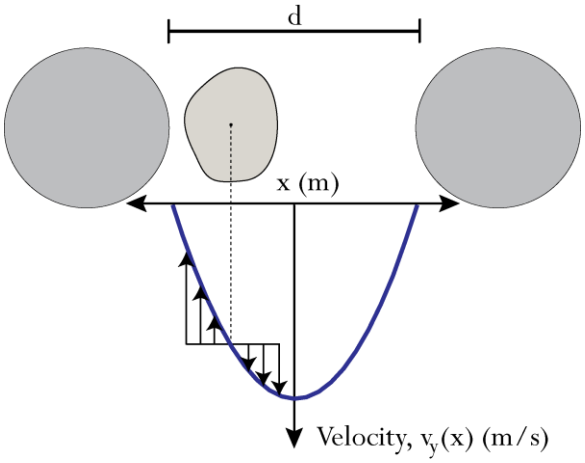


**Fig. 15.** Illustrates how the parabolic flow profile, which relates to the geometry as $v_y(x) = v_{ymax}\left[1 - \left(\frac{x}{d/2}\right)^2\right]$, is linked to the viscous drag acting on a particle.

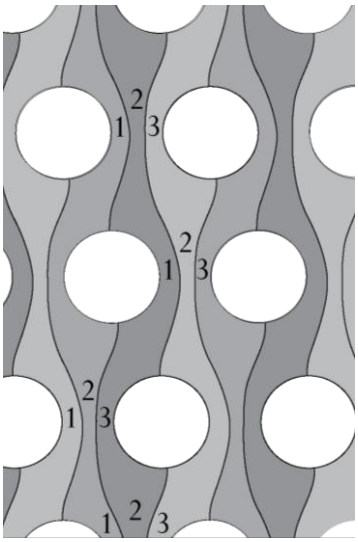


**Fig. 14.** Illustrates flow lanes along the array

Irregular particles can be affected by the parabolic flow profile in the DLD in different ways depending on which mode a particle is in; if in displacement mode, particles tend to rotate continuously (or *flip*) due to asymmetric viscous drag as depicted in fig. 16A but if the particle is in zigzag mode it will not rotate in the same sense because the effective shear (that the particle experiences) is changing continuously as it passes between flow lanes. Rigid sphere-like particles are likely to flip in displacement mode as well but this cannot be seen due to the symmetric nature of a (homochromatic) sphere.

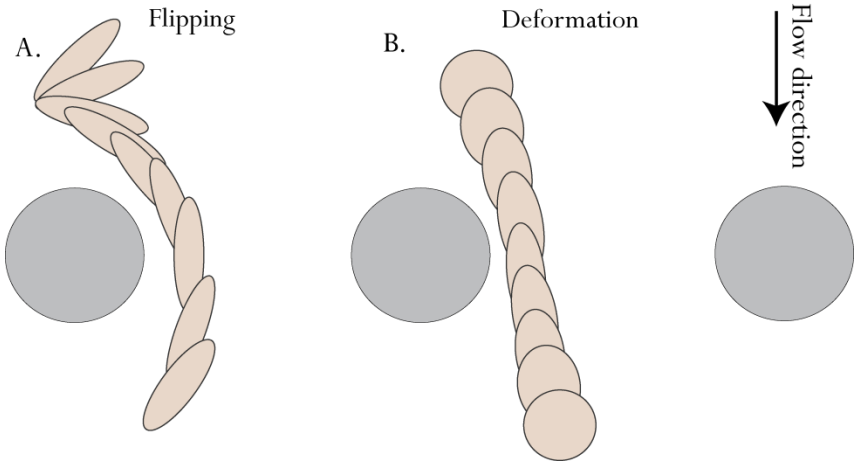


**Fig. 16.** Illustrates how the parabolic flow profile results in asymmetric viscous drag acting on: (A) an irregular particle (B) a soft particle.

If the particle is deformable (and in displacement mode) components of both deformation and flipping influence its behavior in the DLD and shear rate, deformability and relaxation time determines what behavior is dominating. As mentioned, flipping is mostly observed in displacement mode because the net rotational force acting on a particle travelling through all lanes during a period in zig-zag mode is zero. If the period length, N, is very high one might expect to see flipping as well but the particle would change rotational direction after approximately N/2 rows.

Device designs often involve many sections associated with different critical radii through the length of the array (a *chirped* device) which consequently allows for distinction between many different particle sizes[2]. Normally it is crucial to have quite a good idea about what size ranges and critical radii to use for a given particle type in order to create a device from which relevant results can be drawn. However, it has been shown that devices composed entirely out of polydimethylsiloxane (PDMS) can be stretched to change the *dynamic range*[19].

The *critical radius,* which constitute the threshold value between displacement mode and zig-zag mode (as mentioned), has recently been estimated by John A. Davis based on experimental data of a range of different devices[20], resulting in

$$D_C = 1.4 \cdot d \cdot N^{-0.48} \quad (4)$$

where $D_C$ is the critical diameter, d, the gap between laterally adjacent posts and $N$, the period.

### 3.2.1 Erythrocytes in the DLD

Conventional blood diagnostics involve automated counters (*flow cytometry*) in order to measure erythrocyte indices. Flow cytometry setups are expensive and the practice is time consuming, considering sample transport to labs and queues for processing, but is often necessary to assess the many possible causes that manifests as anemia and makes diagnostics non trivial.

The morphologic distributions of *erythrocyte* populations are often more informative than a simple "presence or non-presence" or elevated/decreased levels of a marker of interest. Single cell measurements, like flow cytometry, require that individual cells are measured independently and a separation principle with high resolution and high throughput without compromising cell membrane integrity is essential.

Many physical properties of red blood cells have already been studied because these are closely related to cell function, but because deformability is influenced by a wide range of parameters and intricate interactions involving many structural proteins, membrane dynamics of RBCs is still not fully understood. Many simulation-models have been proposed to deal with the complex dynamics[21, 22].

In contrast to some microfluidics devices, the DLD does not rely on diffusion to work (which the name implies) and diffusion rather impairs resolution. Diffusion in the DLD is not necessarily trivial and is believed to be anisotropic with respect to flow mode of particles resulting in asymmetric distribution broadening[23] and consequently something one would like to minimize. For large particles such as cells, and at realistic fluid flows, diffusion doesn't influence the outcome to any significant extent. A simple Matlab-simulation (Matlab R2009b, the Mathworks, Inc., Natick, Massachusetts, United States) of diffusion for a 5 micron particle in different modes can be seen in fig.17.

As mentioned, the DLD separates particles based on hydrodynamic radius and assymetric particles tend to align so that the smallest geometrical dimension is measured which in the case

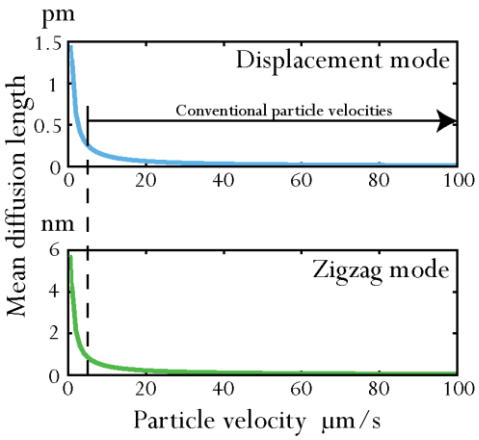


**Fig.17.** Simple Matlab-simulation (Intel Pentium 4 CPU 3.60 GHz, 1GB RAM) to study diffusion for 5μm particles (after $2 \cdot 10^3$ posts with 10μm gaps) in different DLD modes, assuming anisotropic diffusion. Diffusion time in displacement mode is set equivalent to the time a particle spends between two rows and conversely diffusion time in zig zag mode is set as the total amount of time a particle spends in the array.

of erythrocytes means that the "thickness" is the discriminating parameter although Holm and Beech *et al* showed how erythrocytes could be forced to align so that the larger diameter is measured by using a shallow device[14] (see fig. 18). Based on this principle, different geometrical aspects of irregular particles, such as discocytes, can be measured. Also since erythrocytes are higly deformable, components of both flipping (if in displacement mode) and elongation may influence the rheology (as discussed for soft particles in *3.2 Principles of deterministic lateral displacement*, p13-14 ).

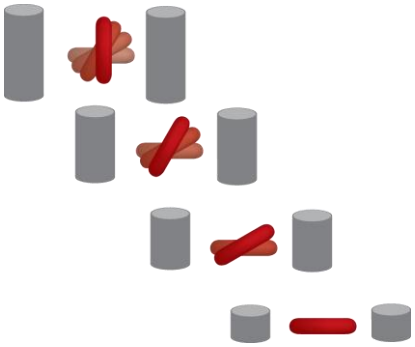

**Fig.18.** A sketch illustrating erythrocyte alignment at different depths.

# 3.3 Experimental setup and method

## 3.3.1 Fabrication process

A master for replica molding was created[vi] using UV-lithography to outline device dimensions in SU-8 resist on a silicon wafer.

PDMS (Sylgard, Dow Corning, Midland, MI, USA) mixed with curing agent in proportions 10:1 was degased for 20 min and poured on to a master followed by 50 min of baking at 80°C, allowing the PDMS to harden. The hardened PDMS was treated with oxygen plasma (plasma preen, Plasmatic systems, Inc, North Brunswick, NJ) to create proximal Si-O termination thus facilitating PDMS-PDMS binding (between channels and bottom plates) and hydrophobicity. In order to prevent sticking and preserve hydrophobicity, PLL-PEG was added to the reservoirs directly after oxygen plasma treatment (for a more detailed description of the fabrication process see *7.1 Lab schemes: Protocol for device fabrication,* p37).

## 3.3.2 Material

The device dimensions are seen in fig. 19 (page 16). The critical diameters range from 1µm in section 1 to 4.5µm in section 8. Buffer inlets on both sides of the sample inlet (C) provide means to focus sample solutions into a narrow stream thus promoting identical conditions for all particles. Depending on displacement, cells/particles are collected in one of the three outlets which allow for further analysis of the separated cells. As mentioned, the entire device was made in PDMS (see *2.3.1 PDMS,* p8).

A pressure regulator (Fluigent, Paris, max 1000 mBar ± 10mBar) was used to drive fluid through the device and, generally, bright field microscopy with a Nikon 4x objective (and a Luca CCD camera handled with Andor IQ software, Andor Technology, Belfast, Northern Ireland) was used to capture videos and evaluate the devices.

A FACScalibur flow cytometer (FACSCalibur, Becton-Dickinson, Franklin Lakes, New Jersey, U.S.) was used in all FACS experiment.

[vi] The masters used for replica molding were made by Jason Beech and Stefan Holm

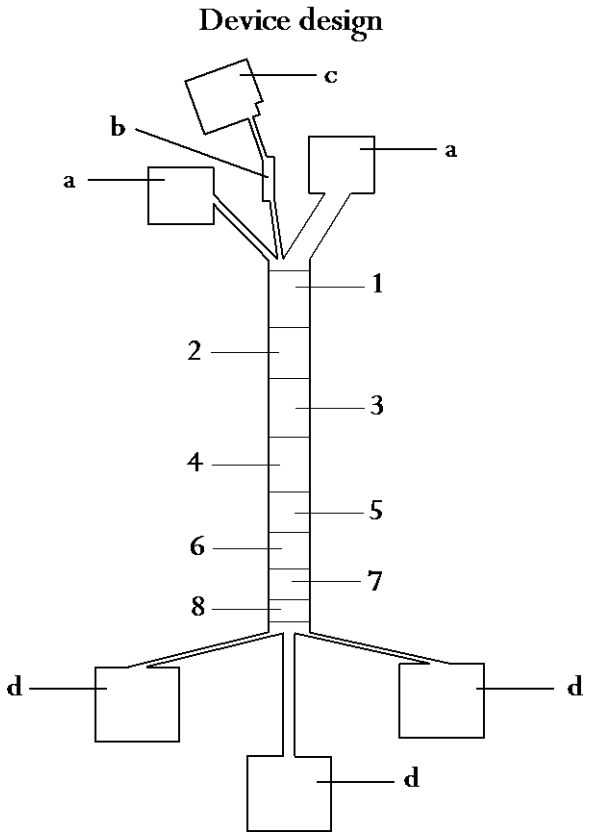


**Fig. 19.**A schematic of the device used in the experiments (see table 5 for device parameters).

### 3.3.3 Cell handling

Discocyte samples for DLD (and FACS) experiments consisted of fresh peripheral venous blood (finger prick) suspended in chilled autoMACS (in proportions 1:6). Experiments with abnormal morphologies[vii] involved an additional step of adding of Triton X-100 to produce stomatocytes or sodium salicylate to produce echinocytes (see fig. 21). Fixated cells (glutaraldehyde) were also investigated as described in appendix (see *7.1 Lab schemes: Discocyte fixation protocol,* p39). Blood samples were taken from the same individual throughout all DLD experiments and from two individuals in the FACS experiments (for more information about lab protocols, see *7.1 Lab schemes,* p37-39).

### 3.3.4 Data evaluation

In order to study outcome distributions in the DLD, videos were taken from the area between section 8 and the outlets (see fig. 19 and fig. 20). Videos were processed in ImageJ (ImageJ, US national Institute of health, Maryland USA) (signal to noise enhancements) and counted with a particle tracker (developed by Stefan Holm) in Matlab.

| Device Parameters | | |
|---|---|---|
| Region | N | CritD* |
| 1 | 65.3 | ~1.13 $\mu m$ |
| 2 | 32.5 | ~1.58 $\mu m$ |
| 3 | 18.5 | ~2.07 $\mu m$ |
| 4 | 13.0 | ~2.45 $\mu m$ |
| 5 | 8.7 | ~2.98 $\mu m$ |
| 6 | 6.2 | ~3.50 $\mu m$ |
| 7 | 4.6 | ~4.02 $\mu m$ |
| 8 | 3.7 | ~4.47 $\mu m$ |
| a | | Buffer inlets |
| b | | Sample filter |
| c | | Sample inlet |
| d | | Outlets |
| Gap between posts (d) | | 6$\mu m$ |
| Depth | | 4.5 or 10.5$\mu m$ |
| Post diameter | | 20 $\mu m$ |

**Table. 5.** Components and regions of separation related to fig.19 (*calculated with eq .4 and refers to rigid sphere-like particles).

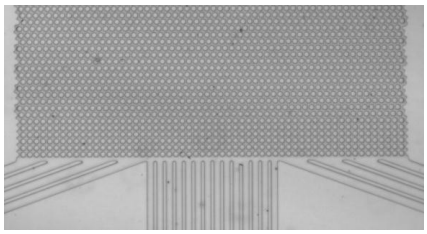

**Fig. 20.** The region by the outlets where videos to evaluate DLD results were taken.

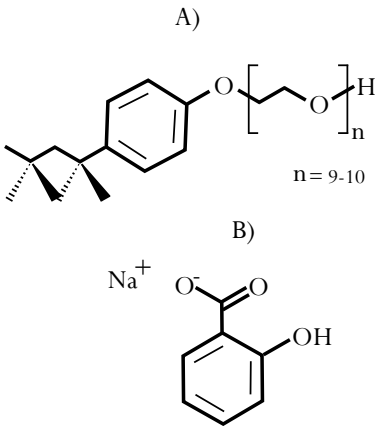


**Fig. 21.** A)Triton X-100[viii] and B)Salicylate.

[vii] Suitable concentrations was determined by studying concentration dependency of transformation (see the results section).
[viii] Based on product specifications from Sigma-Aldrich.

### 3.3.5 DLD experiments

*(See Appendices for detailed descriptions of experimental protocols)*

Cell samples containing erythrocytes of different morphologies (see *3.3.3 Cell handling,* p16) were prepared from fresh peripheral venous blood just before experiments were conducted. Because of the strong influence of buffer composition on morphology, experiments were carried out one erythrocyte species at a time. Before each measurement, PLL-PEG was driven through the device to avoid sticking of plasma proteins and blood cells. Shear-dependent displacement was studied by varying pressure from 100 mbar (from 200 mbar in the 4.5 micron device) to 1100 mbar and results from devices with identical parameters but of different depths (4.5 micron and 10.5 micron) was compared.

### 3.3.6 FACS experiments

Erythrocytes with morphologies identical to those used in the DLD experiments (with the exception of one additional sample containing fixated discocytes), were prepared in quantities of $10^6$ cells in 1 ml samples to avoid saturation and ensure single cell measurements (*general FACS protocols, as were used in these experiments, can be found in the literature and are not presented here*).

# 4 Results

## 4.1 Erythrocyte morphologies

Bright field and SEM images of erythrocytes with different morphologies are presented in figures 22-30 (for SEM preparation protocols, see *Appendix*).

### Discocytes

SEM images (electron microscopy)

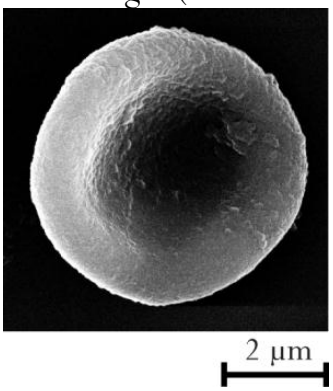


**Fig. 22.** SEM image of discocytes (sputtered with chrome).

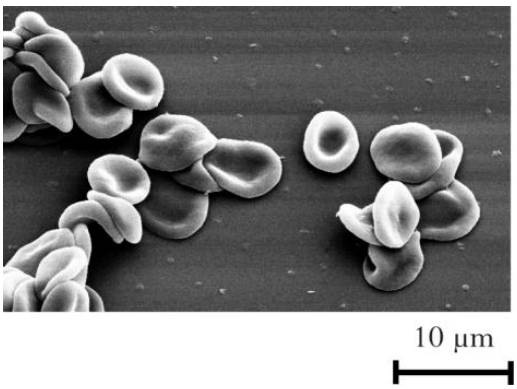


**Fig. 23.** SEM image of discocytes (sputtered with chrome).

Bright field (optical microscopy)

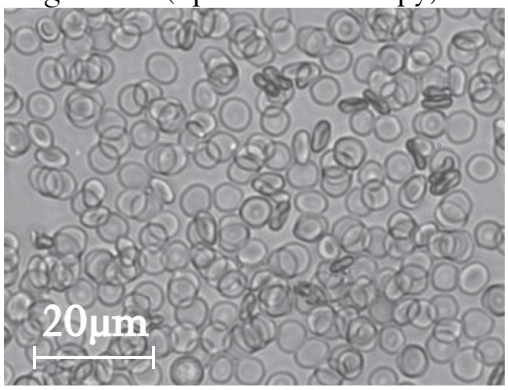


**Fig. 24.** Bright field image of discocytes.

### Echinocytes (Sodium Salicylate)

SEM images (electron microscopy)

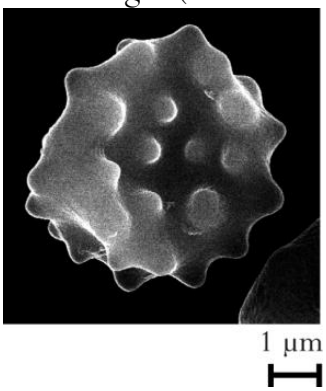


**Fig. 25.** SEM image of an echinocytes (sodium salicylate, sputtered with chrome)

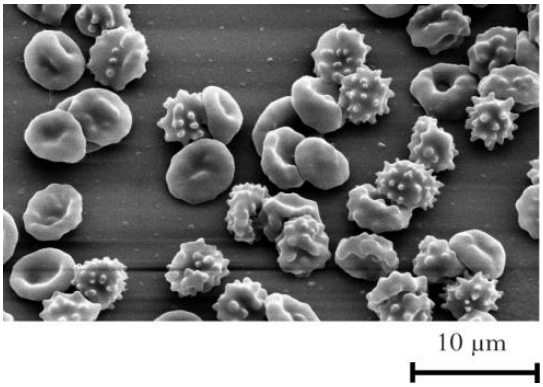


**Fig. 26.** SEM image of erythrocytes, after addition of sodium salicylate, displaying non uniform echinocytic-transformation (sputtered with chrome).

Bright field (optical microscopy)

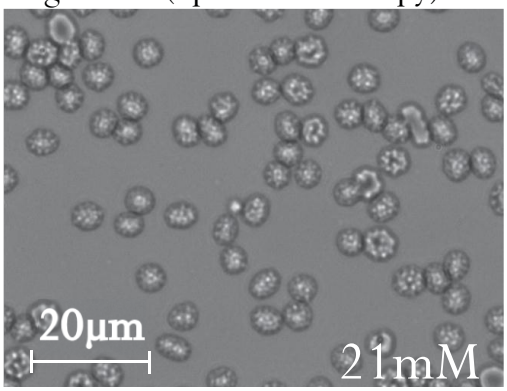


**Fig. 27.** Bright field image of echinocytes in 21 mM sodium salicylate.

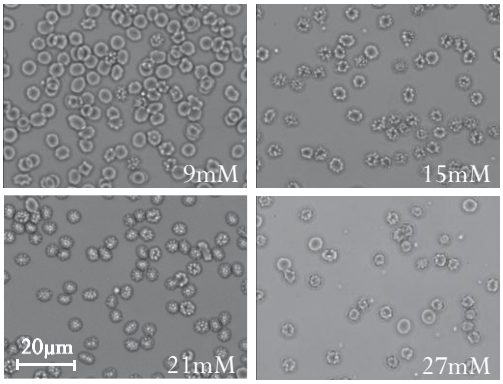


**Fig. 28.** Concentration dependence (sodium salicylate) of echinocytic-transformation.

# Stomatocytes (Triton X-100)

SEM images (electron microscopy)

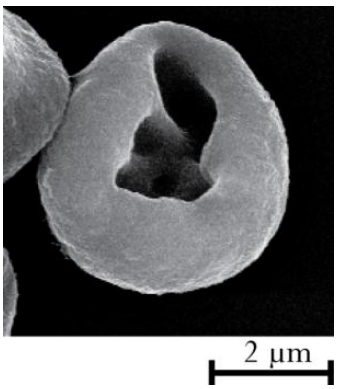


**Fig. 29.** SEM image of a stomatocyte (Triton X-100, sputtered with chrome).

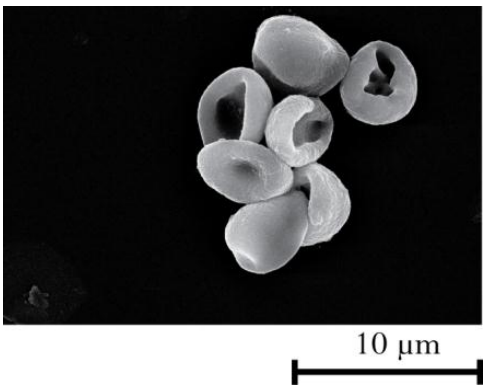


**Fig. 30.** SEM image of stomatocytes, after addition of Triton X-100, displaying non uniform echinocytic-transformation (sputtered with chrome).

Bright field (optical microscopy)

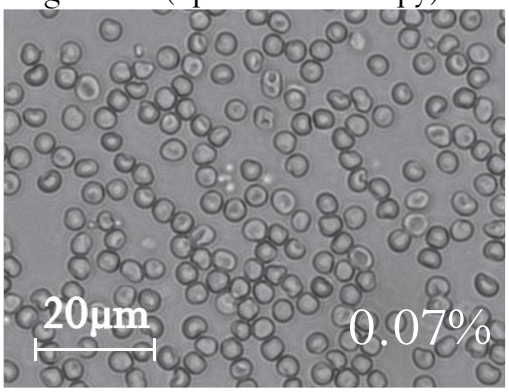


**Fig. 31.** Bright field image of stomatocytes in 0.07% Triton X-100.

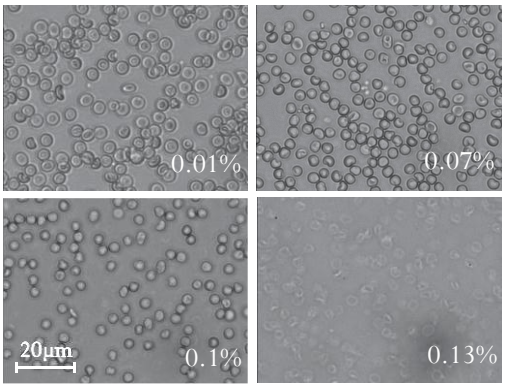


**Fig. 32.** Concentration dependence of stomatocytic-transformation.

## 4.2 DLD results

The results from the DLD experiments (described in *3.3.5 DLD experiments*) are presented in fig. 33-36 (theoretical rigid sphere diameters are calculated with eq. 4).

### 4.2.1 Discocytes

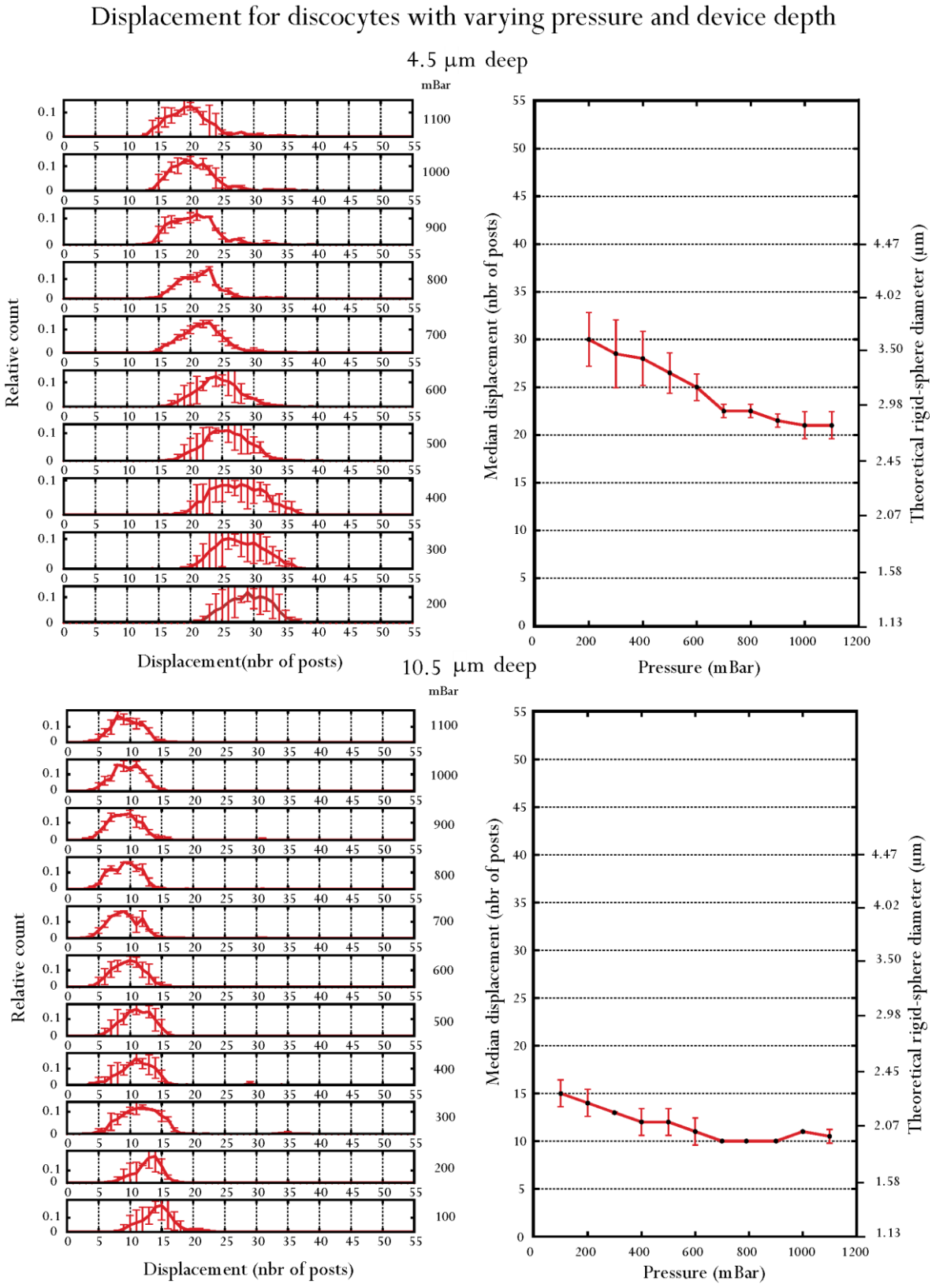


**Fig. 33.** Displacement distributions of discocytes with varying pressure in a 4.5$\mu m$ and a 10.5$\mu m$ device respectively.

### 4.2.2 Echinocytes

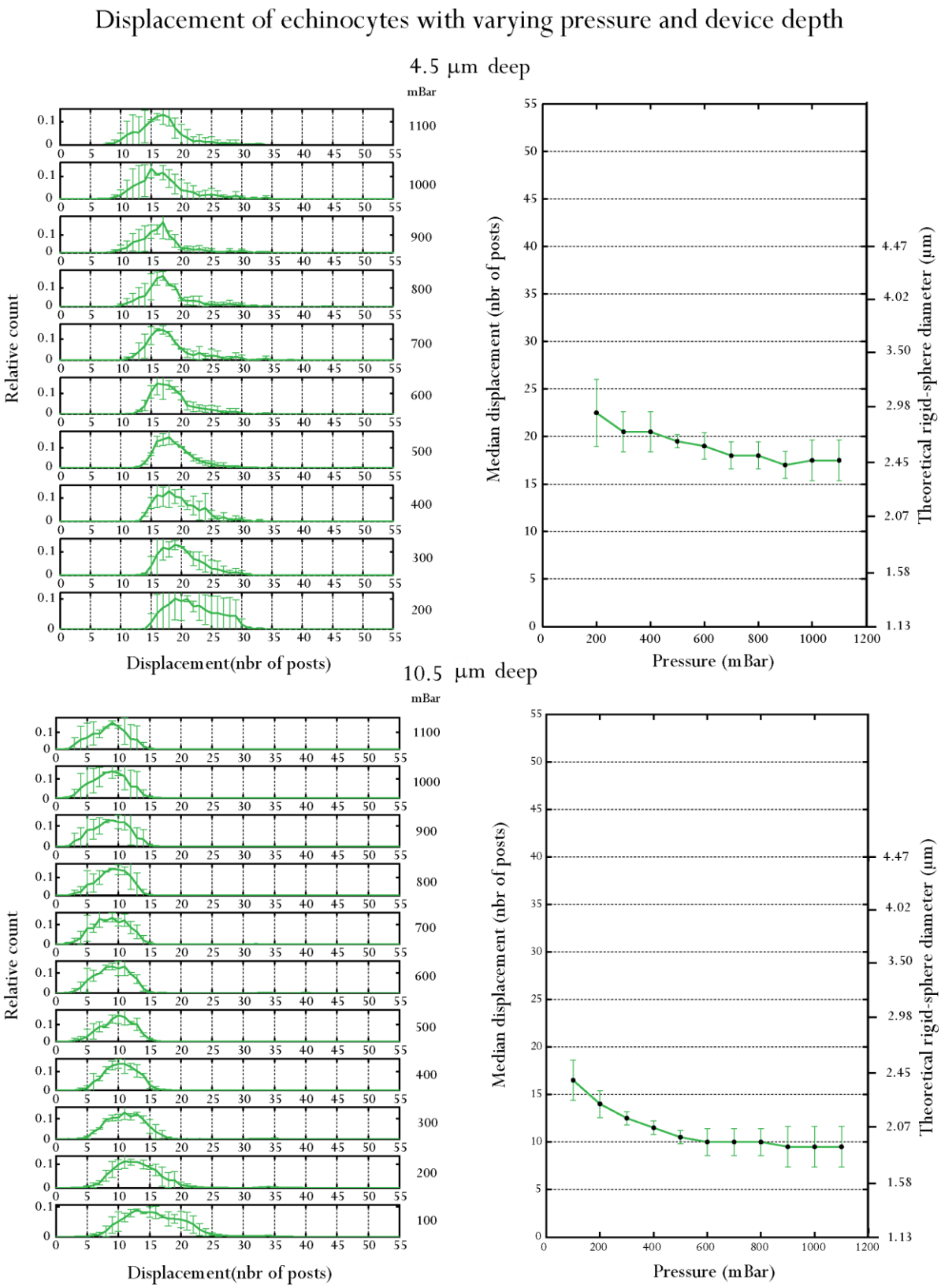


**Fig. 34.** Displacement distributions of echinocytes with varying pressure in a 4.5$\mu m$ and a 10.5$\mu m$ device respectively.

### 4.2.3 Stomatocytes

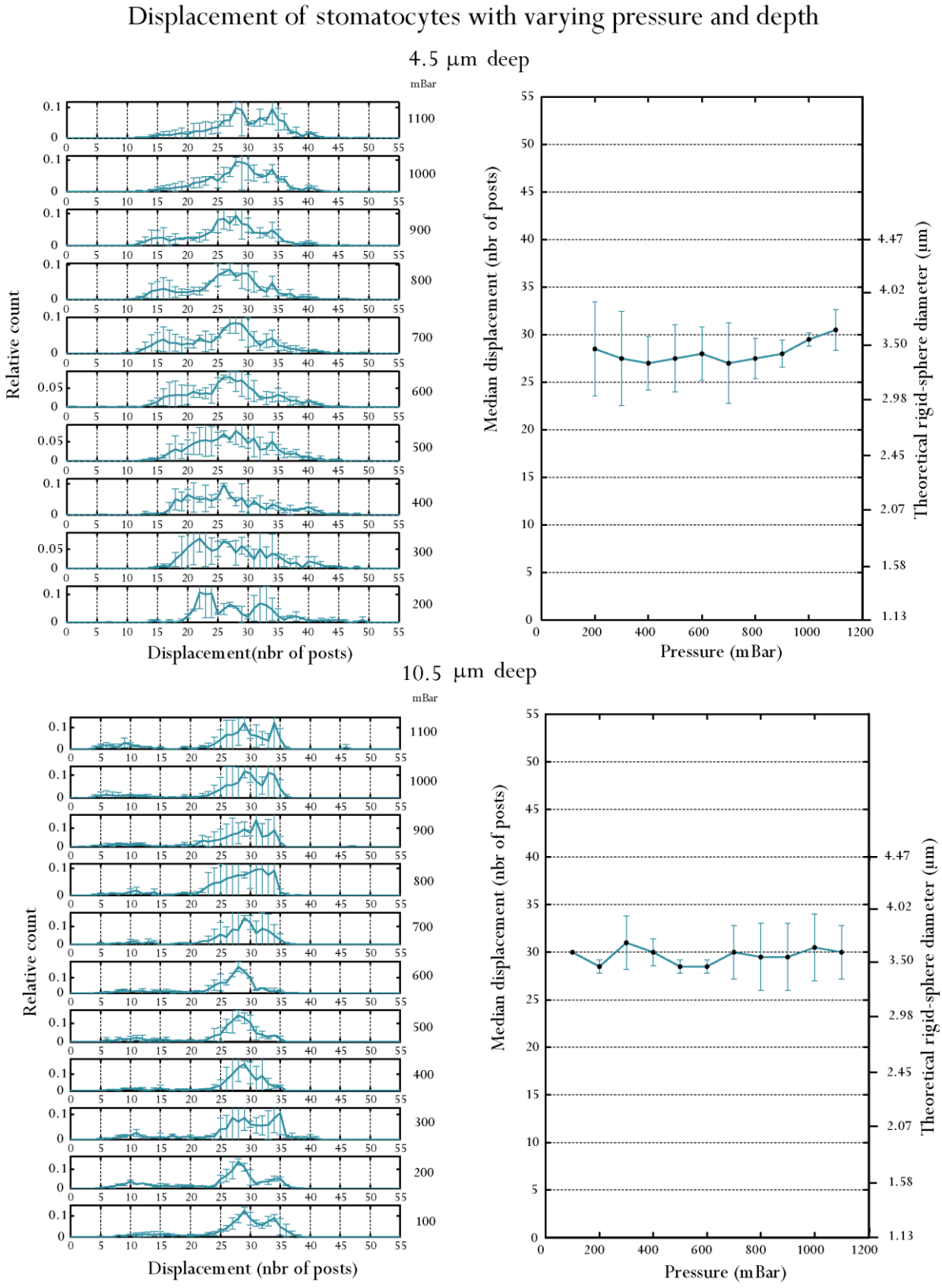


**Fig. 35.** Displacement distributions of Stomatocytes with varying pressure in a 4.5$\mu m$ and a 10.5$\mu m$ device respectively.

## Summary of the experimental results:

Displacement for erythrocytes of various types with varying pressure and at different depths

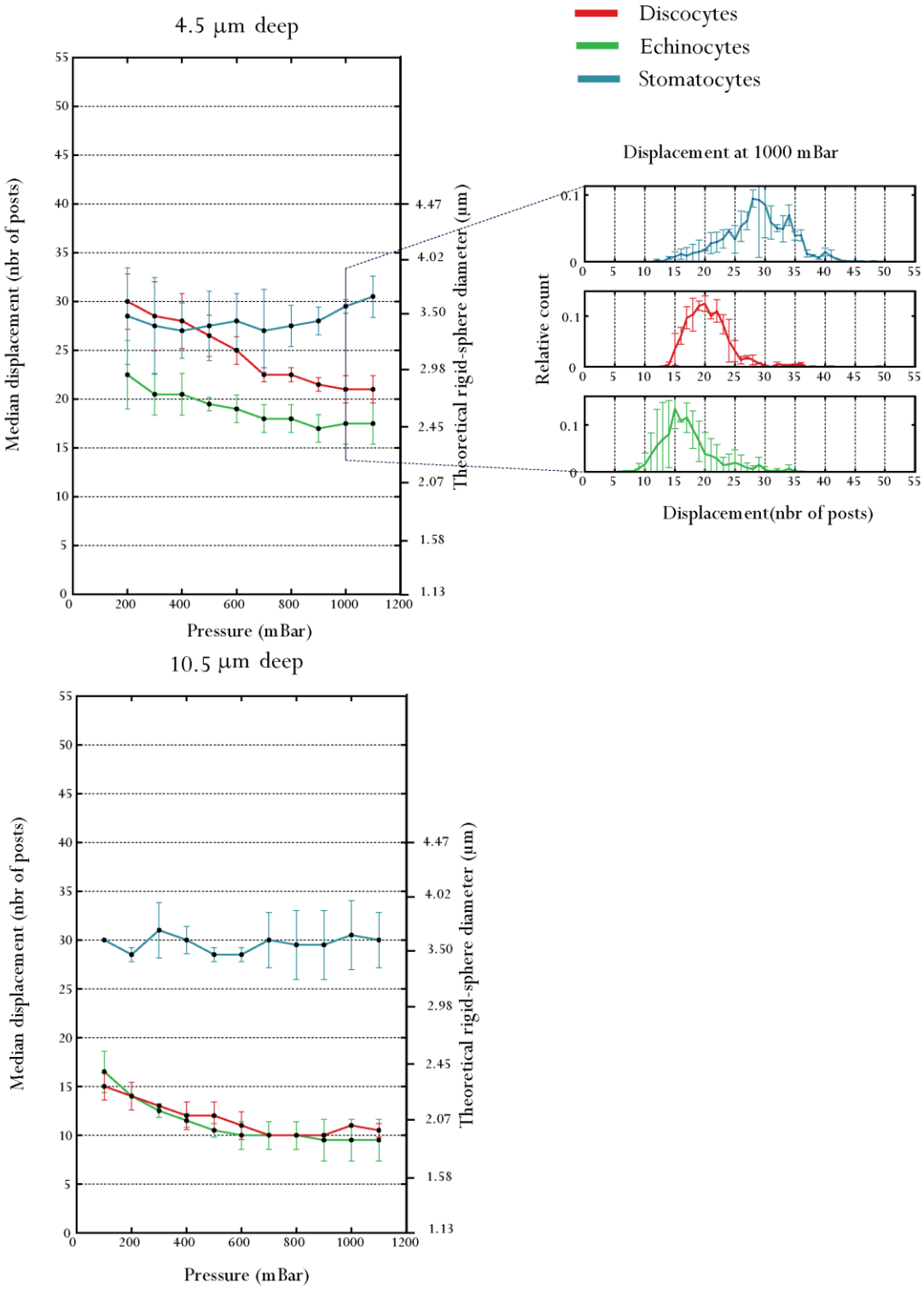


**Fig. 36.** Comparison of DLD results for different erythrocyte morphologies.

## 4.5 FACS results[ix]

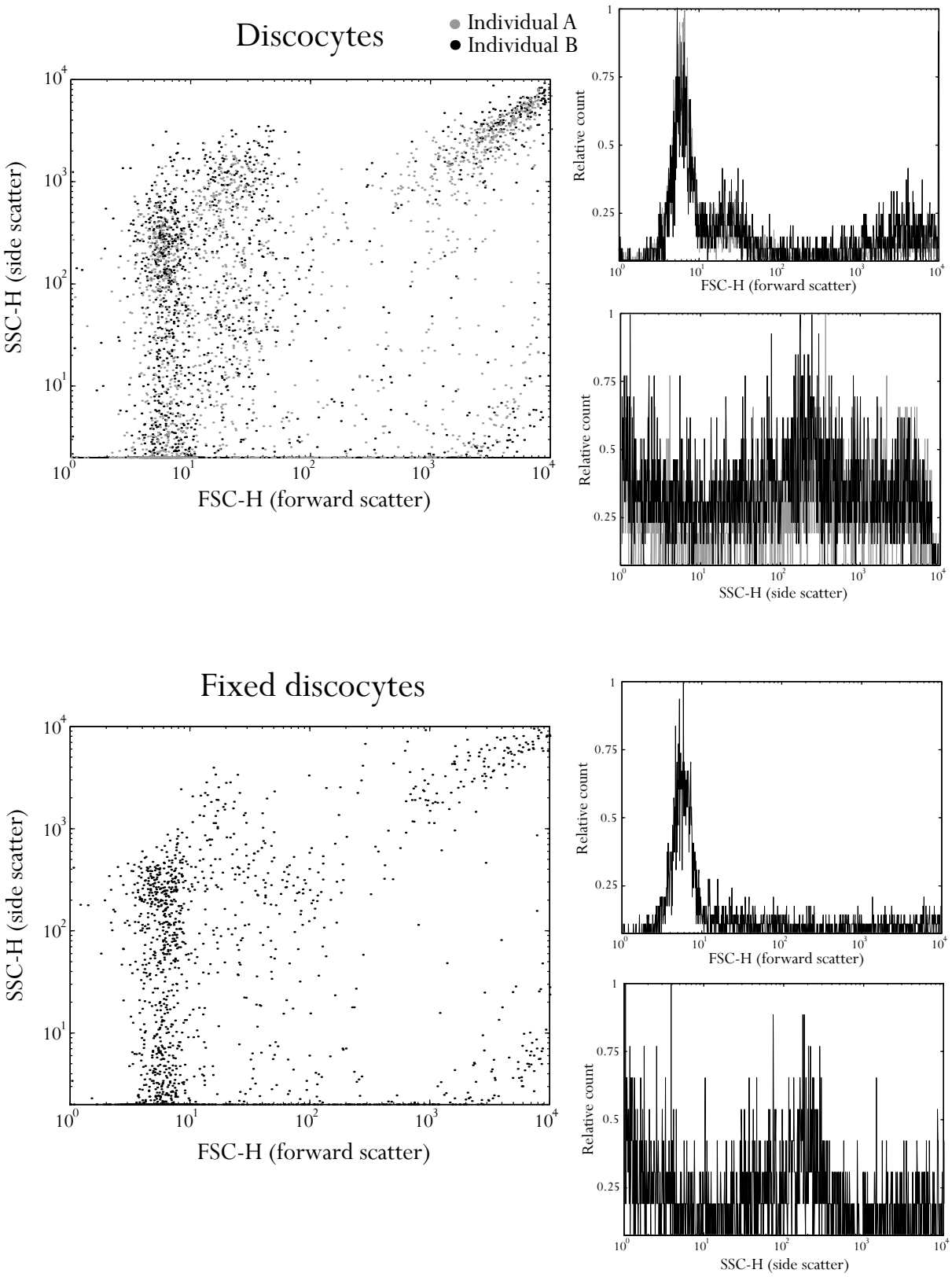


**Fig. 37.** Comparison of FACS results (dot plots and histograms of forward- and side scatter) for fresh and fixated discocytes coming from two individuals.

[ix] Experiments were conducted with a FACScalibur flow cytometer, Becton-Dickinson, Franklin Lakes, New Jersey, U.S.

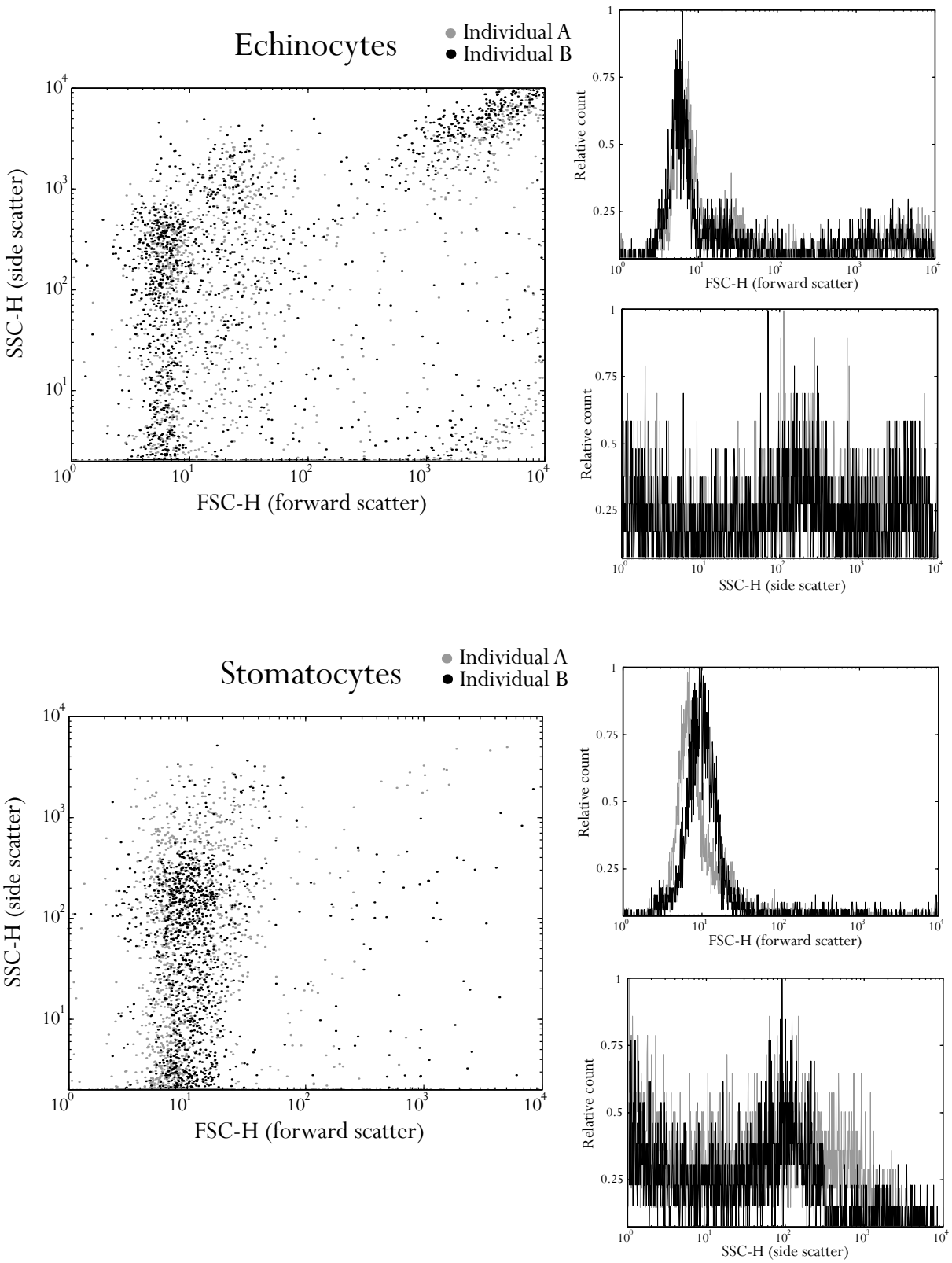


**Fig. 38.** Comparison of FACS results (dot plots and histograms of forward- and side scatter) for echinocytes and stomatocytes coming from two individuals.

# 5 Discussion

## 5.1 Discocytes

In fig. 36 median displacements of all morphologies are compared. Highest separation was obtained in a 4.5$\mu m$ deep device at 1000 mBar and the relative distributions are also shown. The results from fig. 33 show a pronounced pressure (or rather shear-) dependency which suggests that deformability strongly influence discocyte displacement in the DLD. This seems highly likely, based on observations of erythrocyte rheology and especially considering stomatocytes (which are known to be less deformable[24]) do no exhibit shear dependency in the DLD, or at least not in this regime (see fig. 35 and 36). Not taking deformability into account, one would expect the discocytes to appear significantly smaller than the echinocytes and the stomatocytes in the deep device since discocyte thickness is around 2$\mu m$ and the more spherical echinocytes and stomatocytes should appear larger as a result. This is also the case in comparison to stomatocytes but not with echinocytes, it seems, since they exhibit almost identical results in the deep device. The results are beneficial in the context of blood diagnostics because the fact that echinocytes appear smaller in the shallow device and stomatocytes appear larger (than discocytes) it renders both these morphologies detectable as opposed to a situation where both morphologies appear larger.
Due to the difference in depth, and consequently resistance, between the devices (of different depth), shear rate differs considerably. Knowing the shear ratio between the deep and shallow devices at a given pressure is necessary, in order to compare outcome in response to different shear, and it can be roughly estimated since all parameters except the channel height, $h$, are identical

$$\text{shear rate}, \dot{\gamma} = \frac{v}{h} = \left(\frac{1}{h}\right) \cdot \frac{Q}{A} = \left(\frac{1}{h}\right) \cdot \frac{\Delta P}{RA} = \frac{1}{w \cdot h^2} \cdot \frac{\Delta P}{R} \; where \; R \rightarrow \frac{12\eta L}{w \cdot h^3} \; when \; w \gg h$$

$$\rightarrow \dot{\gamma} = \frac{\Delta P h}{12\eta L} \rightarrow \frac{\dot{\gamma}_{deep}}{\dot{\gamma}_{shallow}} \approx \frac{h_{deep}}{h_{shallow}} \approx \frac{10.5\mu m}{4.5\mu m} = 2.3$$

Velocity measurements from recorded particles lead to a shear ratio of approximately 4. Note that this is a crude estimate since particle velocity depends on mode (and lane if in *zig-zag* mode). A displacement-shear graph based on the average value of the two estimations can be seen in fig. 39 below and fig. 42, 43.

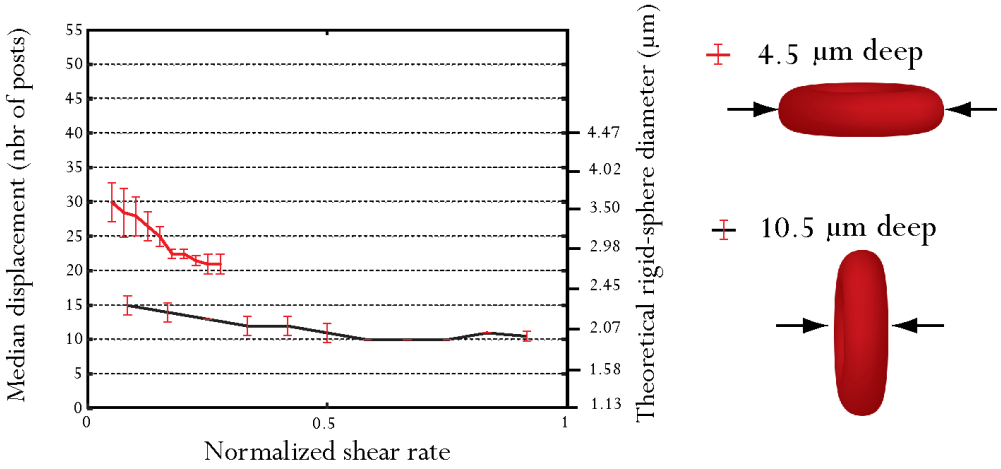


**Fig.39.** Displacement-shear graph for discocytes in varying shear and different device depths.

The discontinuity in the displacement-shear graph (fig. 39) suggest that discocytes are forced to "lie down", in the shallow device, to some extent (as discussed in 3.2.1 *Erythrocytes in the DLD*, p14) which is also supported by visual observations. Measurements with a high speed-camera would be desirable in order to confirm this. This anisotropic response to shear is the case for asymmetric particles (such as discocytes). In contrast, the displacement–shear graph for stomatocytes (fig. 43) does not exhibit the same obvious discontinuation. In other words, the difference between shear plots of different depths is a measure of how spherical a cell (or particle) is,

provided that the Young's modulus is isotropic. This may be equivalent to the *spherical index*[25] associated with flow cytometry (which is essentially the ratio of two scatter peaks resulting from differently oriented erythrocytes) and would be very interesting to investigate further.

Rheinhart *et al*. showed how echinocytes (induced with sodium salicylate) are more deformable than discocytes (and results in higher blood viscosity)[24] and stomatocytes were less deformable than discocytes. The explanation given was that excess cell membrane renders erythrocytes more deformable which supports our view that deformability analysis in the DLD (by varying shear) may give a measure of the ratio between leaflets in the bi-layer and consequently indicate the extent of echinocytosis or stomatocytosis.

Micro filter resistance measurements, as used in the mentioned article (Rheinhart *et al*.[24]), is perhaps the most common approach to determine deformability of cells (i.e. ectacytometry) even though filters are prone to clog[26], resulting in altered pore sizes and consequently altered resistance. The DLD does not clog as easily and is based on an individualistic principle which means that subpopulations based on deformability can be distinguished as opposed to filtering resistance measurements based on bulk behavior. Scatter analysis with sheath flow focusing has been proposed[27] to assess deformability, as well, but this technique is far less versatile and not as simple as DLD.

A number of factors influence deformability such as; cytosolic viscosity (influenced by osmolarity and more), rigidity of the cell membrane, inner supportive structures (e.g. cytoskeleton) and the viscosity of the buffer. The relative influence of parameters may even change depending on shear rate and strength, cell orientation or after plastic deformation. In other words, cell rheology in the DLD (and in microfluidics in general), is quite complex and consequently difficult to deal with analytically. Efforts were made to separate deformability from morphology as an outcome determinant by trying to conduct identical experiments with discocytes fixated in glutaraldehyde. The fixated cells clustered together and were stickier than non-fixated cells which made it impossible to conduct experiments due to clogging as seen in fig. 40 and fig. 41. It would perhaps be feasible if cells were sonicated in advance and if the gap between posts, d, was made larger.

The (non-fixated) discocytes constitute the only, clinically, reliable population evaluated in the report since no altering chemicals were added and the cells were kept in an *in vivo* like milieu. This being said, it is our belief that much of the discriminating properties of the DLD, when dealing with erythrocytes, can be understood by studying DLD outcome for cells with altered membrane morphology and deformability.

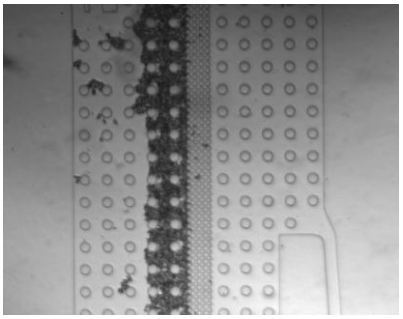

**Fig. 40.** Clogged DLD filter with fixated discocytes (10.5$\mu m$ deep device).

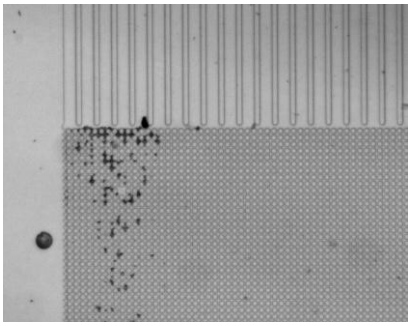

**Fig. 41.** Clogged array with fixated discocytes (10.5$\mu m$ deep device).

# 5. 2 Induced morphologies

Using hypotonic or hypertonic buffers to facilitate morphology alterations was thought to add too many unknown variables since *in vivo* osmolarity in disease states are commonly isotonic (approximately 300 mOsm/l)[15]. Therefore echinocytic- and stomatocytic agents were used in order to produce as clinically relevant morphologies as possible (without having access to pathologic blood) as discussed in *3.1.2 Bilayer-couple theory* on page 11. Unfortunately, osmolarity measurements were never carried out because osmometers were not available but calculations (neglecting cross-reactivity) suggest in vivo like osmolarity. There are however disease states where osmolarity alterations occur and these are normally coupled to renal-liver failure and thus osmolarity induced shapes would be interesting to study in the DLD as well.

In the echinocyte and stomatocyte samples, a small but significant subpopulation of discocytes are present and this fraction of the population always seem to remain as discocytes (see *4.1 Erythrocyte morphologies*). This may explain apparent subpopulations in the displacement distributions of these morphologies. The concentration dependency of echinocytic transformation (as seen in fig. 28) indicate that the transformation is not uniform either, that is, some cells are affected at lower concentrations than others suggesting that there are subpopulations which are more susceptible to echinocytic or stomatocytic transformation (as seen in fig. 32). A possible explanation to these discrepancies may involve a subpopulation known as reticulocytes, which are young erythrocytes (with some remnant organelles and r-RNA[18]) and it is possible that these cells respond differently to these chemicals based on their distinct features. If this is the case, the reticulocyte fraction could be detected in the DLD by adding, for example triton X-100 and would provide valuable information of the bodily response to anemia. Shear-displacement graphs for echinocytes and stomatocytes with shear scaling equivalent to that in fig. 39 are seen in fig.42 and fig.43 respectively.

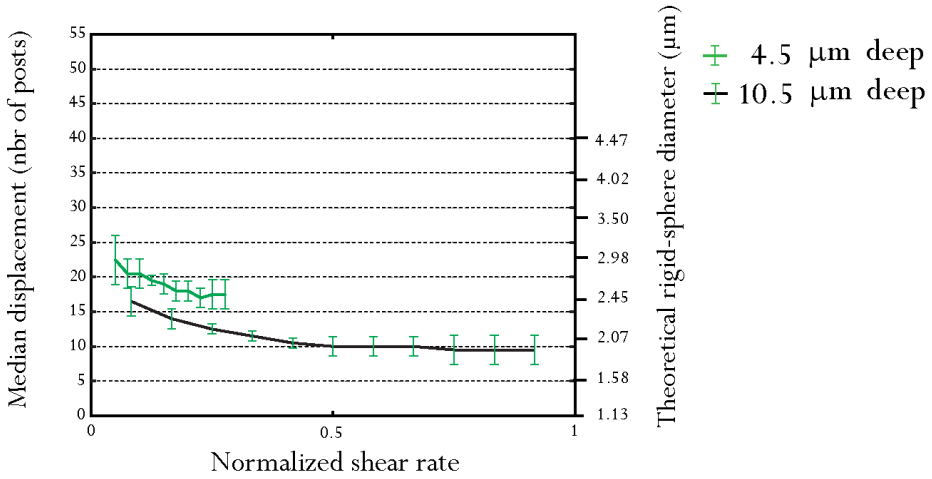


**Fig.42.** Displacement-shear graph for echinocytes in varying shear and different device depths.

The shear-displacement graph for echinocytes (fig. 42) is (as mentioned) more coherent than the corresponding graph for discocytes which is likely due to the more spherical shape of echinocytes (see fig.25-26). Apart from that, echinocytes show similar shear dependency as discocytes suggesting similar deformability.

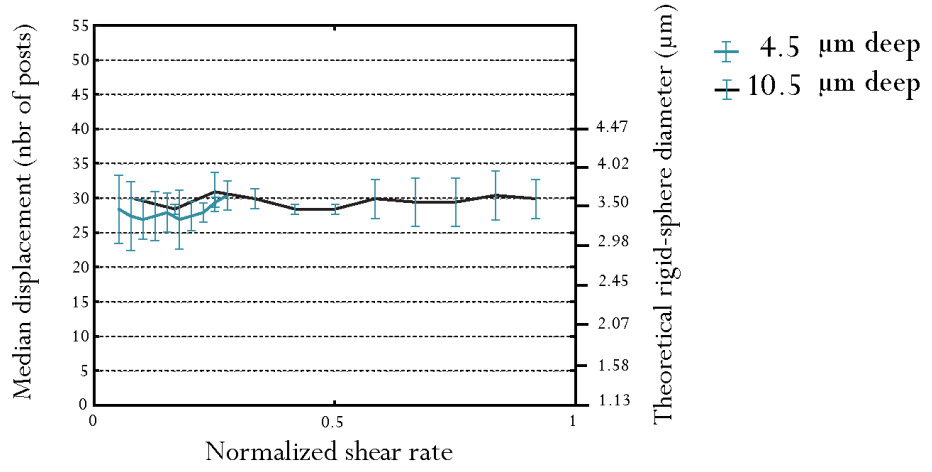


**Fig.43.** Displacement-shear graph for stomatocytes in varying shear and different device depths.

The displacement graph for stomatocytes (fig.43) is not discontinuous (as the case for the other morphologies) which is understandable considering their highly spherical morphology and also, the shear-dependency is fundamentally different (in the studied shear range) indicating similar results to those of Rheinhart *et al*[24]. The standard deviation is higher in the case for stomatocytes (in comparison with other morphologies) which is

interesting as it is indicating an underlying heterogeneity in the sample, but arguably makes the results less reliable. Based on the displacement results in fig. 35 it is likely that the stomatocytes contain a noticeable discocyte subpopulation since a fraction of the cells seems to follow a shear dependency virtually identical to corresponding discocyte distributions (see fig. 44) which consequently influence median displacement graphs. This fraction seems to be somewhat comparable to the amount of discocytes seen in fig.31.

The flipping mode (see *3.2 Principles of deterministic lateral displacement*, p13) is commonly observed for irregular particles like discocytes but not for the more spherical stomatocytes (and echinocytes to some extent). How this, quite distinct behavior, influences DLD outcome in comparison to non-flipping is largely unknown (to the author's knowledge) and would perhaps be interesting to investigate further (see fig.45).

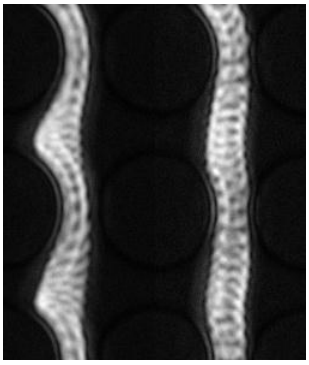

**Fig 45. S**tandard deviation of pixel intensity for flipping (to the left) and non-flipping behavior (right) with $\Delta\lambda = 0$.

## 5.3 Comparison with FACS

Flow cytometry (i.e. FACS) results in fig. 37, 38 and 46 show similar patterns for discocytes and echinocytes though the forward scatter plot suggest somewhat fewer leukocytes and possibly smaller secondary erythrocyte peak which would indicate slightly more spherical shapes. The stomatocytes produce a different pattern and apart from containing very few (if any) viable leukocytes, the erythrocyte peak is not bimodal, which reflects the much more spherical morphology of stomatocytes though it is difficult to evaluate whether mean cell volume have been altered by addition of chemicals.

Side scatter is a measure of inner granularity/complexity and is somewhat equal for all three morphologies which might be expected since the fundamental differences between the cells are rather associated with the membrane. In all it seems stomatocytes are distinguishable in the FACS but not necessarily echinocytes, which is surprising given their distinct appearance (see fig. 25). Isolating the erythrocyte

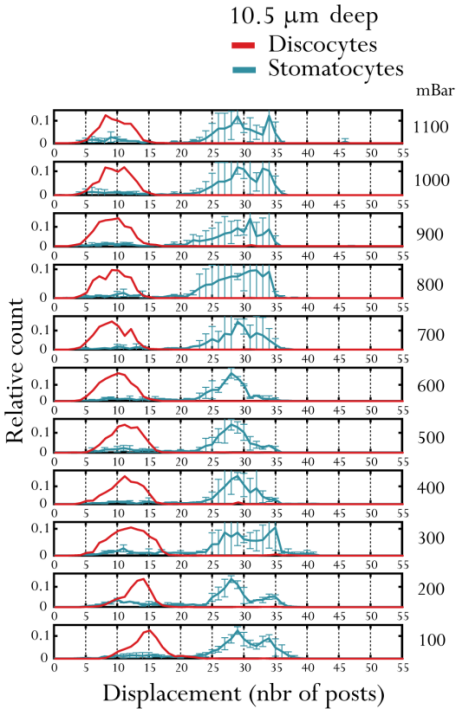


**Fig 44.** Visualizing (what is likely to be) a discocyte subpopulation in the stomatocyte experiments by comparing with discocyte results.

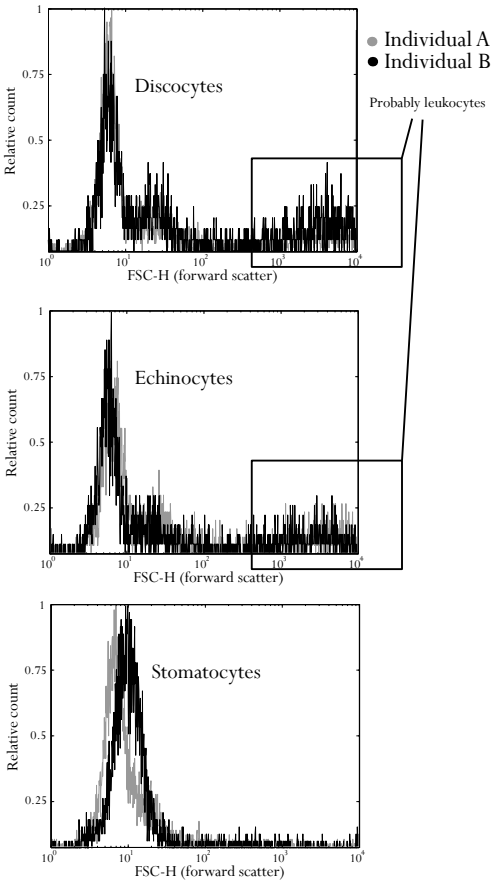


**Fig 46.** Comparison of FACS results for different morphologies.

fraction when analyzing scatter plots from FACS proved surprisingly difficult and a hematologist with FACS experience should probably be involved in future FACS experiments to make the comparison with FACS more informative.

## 5.4 Finite element simulations

Finite element simulations are helpful in understanding, the often complex, flow profiles associated with microfluidics and are perhaps especially useful when studying behavior of soft and/or asymmetric particles which are influenced by shear ($\propto \tau \frac{dv_y}{dx}$). COMSOL-simulations (COMSOL Multiphysics 4.1, COMSOL, Inc, Stockholm, Sweden) of a DLD unit cell, with dimensions similar (not identical) to one of the regions in the device used in this report, are presented in fig.47. By importing the model to Matlab (using LiveLink), criteria such as the flow ratio between side and forward outlets could be met by altering compensatory side pressure using a PID feedback loop (see Appendix for more information). Some simulation parameters are presented in table 6.

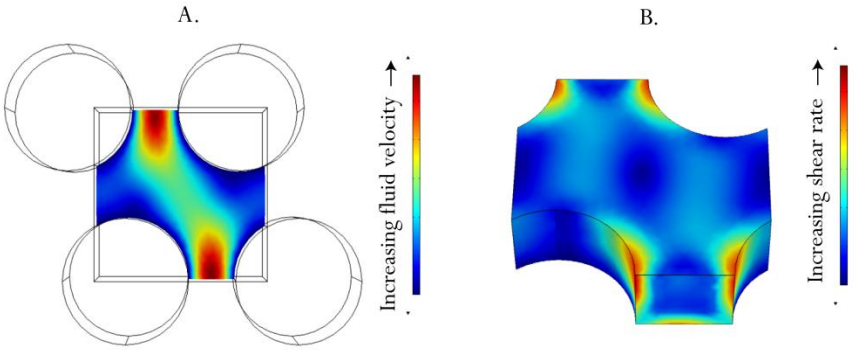


**Fig.47**. Velocity profile (A) and shear rate profile (B) for a unit cell in the DLD (simulation parameters can be seen in table 6).

| Simulation parameters | |
|---|---|
| Post radius | $10\mu m$ |
| d | $10\mu m$ |
| $\lambda$ | $32\mu m$ |
| N | 3 |
| depth | $20\mu m$ |
| Pressure | $100mBar$ |
| L | $32\mu m$ |

**Table 6.** Simulation parameters of a unit cell created to study fluid flow in a DLD device.

A Matlab-program, simulating particle behavior based on a static velocity field (equivalent to the velocity field in fig. 47 A) was developed in order to study influence of different parameters such as particle size and diffusion on DLD outcome, and the results can be seen in fig.48 50.

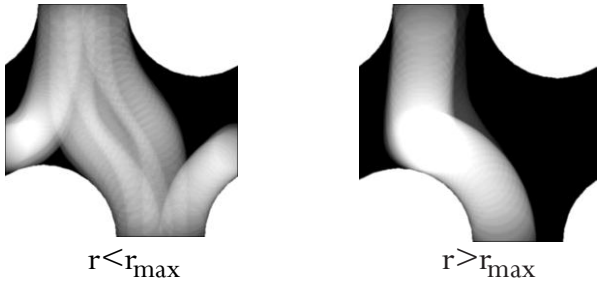


**Fig.48**. Particle trajectories in a unit cell: Zig-zag mode (A) and displacement mode (B)

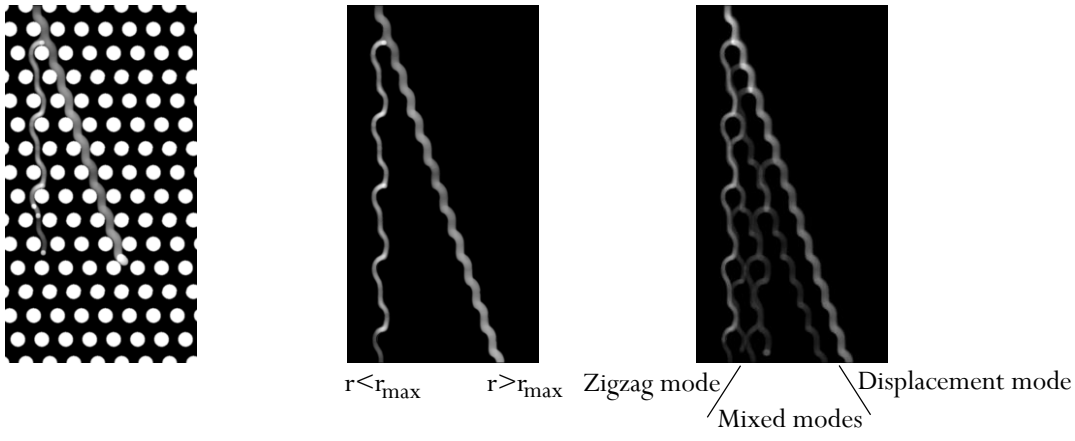


**Fig.49**. Trajectories for particles of different sizes in an array (a result of static velocity field simulations in Matlab).

The COMSOL simulations of velocity and shear landscape as seen in fig. 47 exhibit strong variations and are consistent with the known theory (discussed in *3.2 Principles of deterministic lateral displacement,* p12-13) and thus do not entail new unfamiliar flow behavior coupled to the device design.

Due to time limitations for the thesis, the particle simulations were not developed enough to reflect cell rheology in the DLD realistically (closer to rigid sphere behavior) and it is perhaps better suited for pedagogical purposes though it may prove practical when considering new device designs and to appreciate influence of diffusion (see fig. 50).

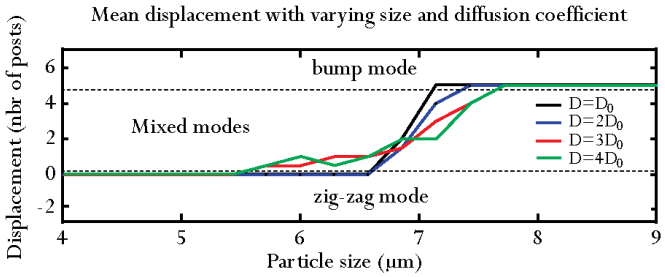


**Fig.50**. Simple particle simulations to study diffusion in mixed modes (diffusivity is set to a constant value for all particle sizes in order to isolate influence of modes). Each graph represents the average values of two simulations.

# 5.5 Conclusions

The results in this report largely mirror the deformability of cells rather than size and morphology though both these parameters could be examined given different values of gap (and period). At low shear, morphology dominates hydrodynamic size and at higher shear, deformability dominates. In other words different parameters can be studied by varying the shear.

Stomatocytes appear larger and echinocytes smaller than discocytes in the 4.5 $\mu m$ deep DLD device which may be used as diagnostic principle for detecting some blood disease states. Also an equivalent to the *spherical index* (associated with FACS) may be obtained by comparing shear-displacement curves at different depths. It is clear that DLD diagnostics allows for analysis of some FACS associated entities (i.e. size and spherical index) and additional parameters, not visible in the FACS. Another beneficial aspect associated with DLD is that cell morphology is, in a sense, evaluated continuously as opposed to FACS which evaluates based on single events and even though faster photodiodes have allowed for higher flow velocities, this constitutes a limitation in terms of throughput and reliability.

The particle-diameter-to-gap ratios in these experiments may be too high to explain behavior based on the classic flow lane theory of DLD, at least in situations where the cells fill the entire width of the gap. In the case of discocytes in a 4.5 $\mu m$ device, the diameter is in the order of 7-8 $\mu m$ which compared to the gap (6 $\mu m$) means that if the discocytes were rigid they would not be able to pass between two adjacent posts and this was confirmed by experiments with fixated discocytes.

This is not the case for normal discocytes however and the flow lane model is still applicable over a certain fluid flow (since the hydrodynamic diameter decreases at higher shear). It may however be more informative to use a device with larger gap and compensate with higher period (N) which would allow cells to pass at lower shear rates and lower deformability resulting in increased dynamic range with respect to deformability.

As discussed, the particular erythrocyte subpopulation that is less susceptible to echinocytic or stomatocytic transformation might be reticulocytes and it would be very interesting to study this group of cells further. It might even be two different subpopulations involved in echinocytic and stomatocytic change respectively.

In order to evaluate the DLD device with less interfering elements, it would be preferable to use parallel channels connected to a single outlet instead of several outlets. Also, a narrower dynamic (size-) range which fit the erythrocytes better would be an enhancement of resolution, perhaps between 2$\mu m$ and 4$\mu m$ (rigid sphere size).

Shear-displacement comparisons between cells in devices of different depths (as in fig. 39 and 42-43) are based on estimations from visual observations of velocity and calculations, and to make more accurate comparisons, one would need to measure the actual flow. This could be solved by using a syringe pump or the use of a flow velocimeter.

Because of the complex nature of hydrodynamic size, when it comes to cells, it would be desirable to study parameters influencing hydrodynamic size independently. An interesting experiment would hence be to involve a fixation step (crossing streams) perhaps in a parallel DLD array which would facilitate cell separation independent of deformability. Also, rigid sphere, tracer-particles would be helpful when comparing experimental results between different DLD device designs.
However, the FACS machine does more than morphology evaluations and can sort based on fluorescence (i.e. fluorescently labeled protein-specific antibodies) and estimate inner granularity.
These features have not yet been coupled to deterministic lateral displacement and a similar setup is probably feasible though the fundamental strength of the DLD lies in that it can discriminate not only based on size but morphology and deformability influencing particles hydrodynamic diameter. More statistics than presented in this report would of course be necessary to confirm clinical relevance of these parameters and experiments would require actual diseased blood rather than artificial states.

## 5.6 Outlook

Mobile phone microscopes will perhaps turn out to be a practical way to study DLD results on "field devices" and facilitate fast information forwarding to experts from places far from medical institutions or possibly diagnosis by means of software. Mobile phone microscopes (fig. 51) have been shown[28] capable of producing a resolution of ~1.2 μm and these kinds of general framing devices are extremely valuable in order to create more and practical diagnostics devices and take microfluidics closer to widespread commercialization.

Current directions of many microfluidic research groups involve putting together larger (complete) systems and there are many possibilities to explore. The versatility of the DLD which is emphasized in this report not only includes conventional separation but also "crossing streams" which allow for staining or chemical reactions whilst continuously separating the resulting products. For these reasons, DLD may very well turn out be a cornerstone of many devices and a proposed setup is presented in fig. 52 (on the next page).
Lastly; it is the author's belief that the DLD could complement the FACS to introduce new interesting variables (especially considering the clinical relevance of erythrocyte deformability) and though some might be of the opinion that there is already too much information to handle coming from the FACS alone, there are alternative (computerized) ways to handle and interpret large amounts of data to deduce clinical indications e.g. with neural network algorithms [29] or genetic programming[30].

**Fig. 51.** Portable, mobile phone microscope[x] to evaluate results from microfluidic devices[28].

[x] Courtesy of Prof. Daniel A. Fletcher, UC Berkeley and Lawrence Berkeley National Laboratory

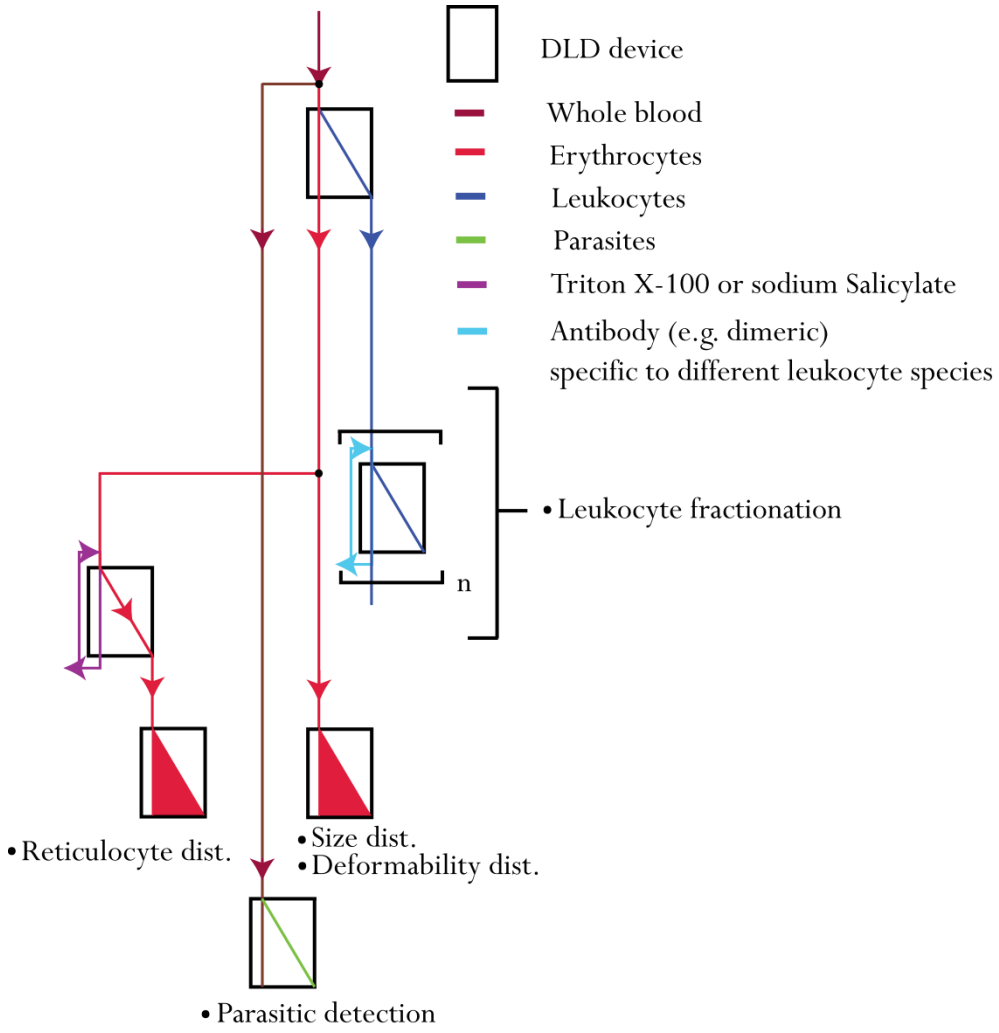


**Fig. 52.** A simple sketch of a setup (i.e. diagnostics system) involving DLD devices with crossing streams and separation steps which may be used to detect many clinically relevant blood indices.

# 6 References


[1] Harold Craighead
*Future lab-on-a-chip technologies for interrogating individual molecules*
*Nature*, Vol 442, 27 July 2006; DOI: 10.1038/nature05061

[2] Lotien Richard Huang, Edward C. Cox, Robert H. Austin, James C. Sturm
*Continuous particle separation through deterministic lateral displacement*
*Science,* no 304, 2004, p 987, DOI: 10.1126/science.1094567

[3] Leonard A. Herzenberg, David Parks, Bita Sahaf, Omar Perez, Mario Roederer and Leonore A. Herzenberg
*The History and Future of the Fluorescence Activated Cell Sorter and Flow Cytometry:A View from Stanford*
*Clinical Chemistry* 48, No. 10, 2002, p1819–1827

[4] E Ch. Mokken , M. Kedaria , Ch. P. Henny , M.R. Hardeman , and A.W. Gelb
*The clinical importance of erythrocyte deformability, a hemorrheological parameter*
*Annals of hematology,* 2004, Vol. 64, Nr 3, p113-122, DOI: 10.1007/BF01697397

[5] John A. Davis , David W. Inglis, Keith J. Morton, David A. Lawrence, Lotien R. Huang, Stephen Y. Chou, James C. Sturm and Robert H. Austin
*Deterministic hydrodynamics: Taking blood apart*
*PNAS*, October 2006 vol. 103 no. 40, p14779-14784, DOI:10.1073/pnas.0605967103

[6] David W. Inglis, Nick Herman, and Graham Vesey
*Highly accurate deterministic lateral displacement device and its application to purification of fungal spores*
*Biomicrofluidics*, 2010 June; 4(2): 024109, DOI: 10.1063/1.3430553.

[7] Siyang Zheng, Raylene Yung, Yu-Chong Tail, Harvey Kasdan
*Deterministic lateral displacement MEMS device for continuous blood separation*
18th IEEE International Conference on MEMS, 2005, p 851-854, DOI:10.1109/MEMSYS.2005.1454063

[8] David Erickson and Dongqing Li
*Integrated microfluidic devices*
*Analytica Chimica Acta,* April 2004, Vol. 507, Issue 1, p11-26, DOI:10.1016/j.aca.2003.09.019

[9] Younan Xia and George M. Whitesides
*Soft lithography*
*Annu. Rev. Mater. Sci.,* 1998, (28), p153-184, DOI: 10.1002/(SICI)1521-3773(19980316)37:5<550

[10] Stephanie Vande Vondele, Janos Vörös, Jeffrey A. Hubbell
*RGD-grafted poly-l-lysine-*graft*-(polyethylene glycol) copolymers block non-specific protein adsorption while promoting cell adhesion*
*Biotechnology and Bioengineering*, Volume 82, June 2003, Issue 7, p784–790, DOI: 10.1002/bit.10625

[11] Helene Andersson and Albert van den Berg
*Microfluidic devices for cellomics: a review*
*Sensors and Actuators*, July 2003, Vol. 92, Issue 3(15), p315-325, DOI:10.1016/S0925-4005(03)00266-1

[12] Toru Kojima, Yuuri Hashimoto, Yuichi Watanabe, Shunsuke Kagawa, Futoshi Uno,Shinji Kuroda, Hiroshi Tazawa, Satoru Kyo, Hiroyuki Mizuguchi, Yasuo Urata, Noriaki Tanaka and Toshiyoshi Fujiwara
*A simple biological imaging system for detecting viable human circulating tumor cells*
*J Clin Invest*., October 2009, Vol. 119(10), p3172–3181, DOI: 10.1172/JCI38609.

[13] Sunitha Nagrath, Lecia V. Sequist, Shyamala Maheswaran, Daphne W. Bell, Daniel Irimia, Lindsey Ulkus, Matthew R. Smith, Eunice L. Kwak, Subba Digumarthy, Alona Muzikansky, Paula Ryan, Ulysses J. Balis, Ronald G. Tompkins, Daniel A. Haber & Mehmet Toner
*Isolation of rare circulating tumour cells in cancer patients by microchip technology*
*Nature,* December 2007, Vol.450, p1235-1239, DOI:10.1038/nature06385

[14] Stefan Holm, Jason Beech, Michael P. Barrett and Jonas Tegenfeldt
*Separation of parasites from human blood using deterministic lateral displacement*
*Lab-chip,* 2011, DOI: 10.1039/C0LC00560F.

[15] Milo *et al*. Nucl. Acids Res., 2010, 38 (suppl 1): D750-D753.
URL: http://bionumbers.hms.harvard.edu/

[16] Thomas E. Andreoli , Charles C. J. Carpenter, Robert C. Griggs, Joseph Loscalzo
*Cecil essentials of medicine*
Saunders, 2004, 6th ed., p431-460, ISBN: 0721601472

[17] Michael P. Sheetz and S. J. Singer
*Biological Membranes as Bilayer Couples. A Molecular Mechanism of Drug-Erythrocyte Interactions*
*PNAS*, November 1974, vol. 71 no. 11, p4457-4461

[18] Yoshihito Yawata
*Cell membrane: the red blood cell as a model*
Wiley-VCH, 2003, p220-250, ISBN10: 3527304630

[19] Jason P. Beech and Jonas O. Tegenfeldt
*Tuneable separation in elastomeric microfluidics devices*
*Lab Chip*, 2008, 8, p657-659, DOI: 10.1039/B719449H

[20]John Alan Davis
*Microfluidic Separation of Blood Components through Deterministic Lateral Displacement*
Doctoral dissertation, Princeton University, Sep.2008, p24

[21]Khaled Khairy and Jonathon Howard
*Minimum-energy vesicle and cell shapes calculated using spherical harmonics parameterization*
*Soft Matter*, 2011, Advance Article, DOI: 10.1039/c0sm01193b

[22]Gerald Lim H. W., Michael Wortis and Ranjan Mukhopadhyay
*Stomatocyte–discocyte–echinocyte sequence of the human red blood cell: Evidence for the bilayer– couple hypothesis from membrane mechanics*
*PNAS*, December 2002, vol. 99 no. 26, p16766-16769, DOI: 10.1073/pnas.202617299

[23] Martin Heller and Henrik Bruus

*A theoretical analysis of the resolution due to diffusion and size dispersion of particles in deterministic lateral displacement device*
*J. Micromech. Microeng*, 2008, Vol. 18, 075030 (6pp), DOI:10.1088/0960-1317/18/7/07503

[24] WH Reinhart and S Chien
*Red cell rheology in stomatocyte-echinocyte transformation: roles of cell geometry and cell shape*
*Blood*, 1986, Vol.67, p1110-1118, PMID: 3955230

[25] M Piagnerelli, K Zouaoui Boudjeltia, D Brohee, *et al*
*Assessment of erythrocyte shape by flow cytometry technique*
*J Clin Pathol*, June 2006, Vol. 60, p549-554, DOI: 10.1136/jcp.2006.037523

[26] Reinhart WH, Usami S, Schmalzer EA, Lee MM, Chien S.
*Evaluation of red blood cell filterability test: influences of pore size, hematocrit level, and flow rate.*
*J Lab Clin Med*. Oct 1984,Vol.104(4),p501-516, PMID: 6481214

[27] Georgios S. Stamatakos, Dido Yova, and Nikolaos K. Uzunoglu
*Integral equation model of light scattering by an oriented monodisperse system of triaxial dielectric ellipsoids: application in ectacytometry*
*Applied Optics*, 1997, Vol. 36, Issue 25, p6503-6512, DOI:10.1364/AO.36.006503

[28] Breslauer DN, Maamari RN, Switz NA, Lam WA, Fletcher DA,
*Mobile Phone Based Clinical Microscopy for Global Health Applications.*
PLoS ONE, 2009, 4(7): e6320, DOI:10.1371/journal.pone.0006320

[29] Forsström JJ, Dalton KJ.
*Artificial neural networks for decision support in clinical medicine.*
*Ann Med.*, Oct 1995, Vol. 27(5), p509-517, PMID: 8541025

[30] Kentala E, Laurikkala J, Pyykkö I, Juhola M.
*Discovering diagnostic rules from a neurotologic database with genetic algorithms.*
*Ann Otol Rhinol Laryngol.*, Oct 1999. Vol. 108(10), p948-954, PMID: 10526849

[31] J. G. G. Dobbe, M. R. Hardeman, G. J. Streekstra, J. Strackee, C. Ince, and C. A. Grimbergen
*Analyzing Red Blood Cell-Deformability Distributions*
*Blood Cells, Molecules, and Diseases,* May/June 2002, Vol. 28(3), p 373–384, DOI:10.1006/bcmd.2002.0528

[32] Barbara J. Bain
*Blood cells: a practical guide*
Wiley-Blackwell, June 2006, p20-74, ISBN: 9781405142656

[33] Robert S. Hillman, Kenneth A. Ault, Henry M. Rinder
*Hematology in clinical practice: a guide to diagnosis and management*
McGraw-Hill Professional, 2005, 4th ed., p 13-15, ISBN: 0-07-144035-6

[34] Jason P. Beech, Peter Jönsson and Jonas O. Tegenfeldt.
*Tipping the balance of deterministic lateral displacement devices using dielectrophoresis*
*Lab chip*, Sep 2009, 9(18), p2698-706; DOI: 10.1039/B823275J

# 7 Appendix

## 7.1 Lab schemes

### Protocol for device fabrication:

*Estimated time: 1.5-2 h*

1. **Mix PDMS**
   - Add 3 g PDMS and 0.3 g hardener to a plate.
   - Mix with a pipette cone for 1 minute.
2. **Put in vacuum chamber for 30 min**
3. **Apply to master**
   - Pour PDMS on the silicon master and attach reservoir tubes on outlets and inlets.
   - Pour PDMS on a glass slide and slide another glass slide on top.
   - Make sure there are no air bubbles between the slides and carefully slide them apart creating a thin layer of PDMS on both or at least one of the glass slides.
   - Incubate all PDMS components in 80°C for 50 min to anneal.
4. **Transfer to glass slide**
   - Transfer the annealed PDMS device to a new glass slide.
   - Puncture the PDMS beneath the reservoir tubes with a syringe and remove the detached PDMS from each inlet/outlet
5. **Plasma treatment**
   - Turn the device on the glass slide (tubes facing downwards).
   - Put the device and the glass slide with a PDMS layer in the oven and turn on valves and power behind the oven.
   - Turn on vacuum pump and let pressure fall to 10mBar
   - Turn on $O_2$, let pressure go up to 100 mBar and run on maximum power for 30s.
   - Turn off $O_2$ and wait for 60s.
   - Turn on $N_2$, let pressure go up to 120 mBar and run on maximum power for 30s.
   - Turn off $N_2$ and wait 60s.
   - Turn off valves and power behind the oven.
   - Open oven and remove devices.
6. **Attach the device on a slide**
   - Carefully place the device on the bottom layer with cavities facing downwards and the middle part touching the PDMS layer first.
   - Cut off excessive PDMS.
7. **Add PLL-PEG**
   - Add PLL-PEG to all outlets.

# Protocol for DLD experiments:

1. **Prepare the device**
    - Add PLL-PEG to all inlets and run through with 20 mbar pressure for 10 min.
2. **Morphology preparations (Only one morphology at a given experiment)**

**Discocytes**
Sample: 100 mul autoMACS, 20 mul blood
Buffer: 200 mul autoMACS

**Echinocytes**
Sample: 100 mul autoMACS, 7mul 0.3M Sodium Salicylate, 20 mul blood
Buffer: 200 mul autoMACS, 14 mul 0.3M Sodium Salicylate

**Stomatocytes**
Sample: 100 mul autoMACS, 1.4 mul 5% Triton X-100, 20 mul blood (Heat 5% Triton solution to 37 degrees before adding to autoMACS)
Buffer: 200 mul autoMACS, 0.8 mul 5% Triton X-100

OBS! IT IS CRITICAL THAT SAMPLE AND BUFFER CONC OF TRITON ARE NOT TOO HIGH, OTHERWISE SPHEROCYTES LYSE WHILE SOME DISCOCYTES DO NOT WHICH CAN PRODUCE MISLEADING RESULTS

3. **Load buffer and sample**
    - Add buffer, connect to pressure gauges (5 mbar)
    - Add sample, , connect to pressure gauge (5 mbar)
    - Make sure sample stream is focused and that overall flow is symmetric.
4. **Take videos**
    - Record videos of cells moving to the outlets in the array with appropriate frame rate, frequency of cells and video length.

## Discocyte fixation protocol

Add 20µl of blood from a finger prick to 180µl of PBS (find out info) chilled in ice, in a 1.5ml eppendorf tube.

- Centrifuge at 600g and 4°C for 10 minutes.
- Remove the supernatant and replace with 180µl of chilled PBS.
- Repeat 2. and 3.
- Repeat 2.
- Add 20µl of 25% glutaraldehyde stock solution to 180µl of chilled PBS.
- Remove supernatant and replace with 180µl of the 2.5% glutaraldehyde solution.
- Leave at room temp for 1 hour.
- Centrifuge at 600g and 4°C for 5 minutes.
- Remove the supernatant and replace with 180µl of chilled PBS.
- Repeat 9. and 10. twice.

## Preparation for SEM (by Jason Beech)

- Centrifuge at 600g and 4°C for 5 minutes.
- Remove supernatant and replace with 100ul 50% etoh and wait ~5mins
- Centrifuge at 600g and 4°C for 5 minutes.
- Remove supernatant and replace with 100ul 70% etoh and wait ~5mins
- Centrifuge at 600g and 4°C for 5 minutes.
- Remove supernatant and replace with 100ul 90% etoh and wait ~5mins
- Centrifuge at 600g and 4°C for 5 minutes.
- Remove supernatant and replace with 100ul 100% etoh and wait ~5mins

Place drop of solution (~2ul) on a polisine slide and allow to dry. Sputter on chrome layer (~10nm?)

## 7.2 Matlab

Due to the extensive amount of coding associated with flow simulations with COMSOL-Matlab LiveLink and particle simulations in Matlab, it is not presented here but can be accessed by sending an email to kalleadolfsson@gmail.com